

Review

# An Overview of the Recent Developments in Carbon Quantum Dots—Promising Nanomaterials for Metal Ion Detection and (Bio)Molecule Sensing

Silvija Šafranko <sup>1</sup>, Dominik Goman <sup>2</sup>, Anamarija Stanković <sup>2</sup>, Martina Medvidović-Kosanović <sup>2</sup>, Tihomir Moslavac <sup>1</sup>, Igor Jerković <sup>3,\*</sup> and Stela Jokić <sup>1,\*</sup>

<sup>1</sup> Faculty of Food Technology Osijek, University of Osijek, Franje Kuhača 18, 31000 Osijek, Croatia; silvija.safranko@ptfos.hr (S.Š.); tihomir.moslavac@ptfos.hr (T.M.)

<sup>2</sup> Department of Chemistry, University of Osijek, Ulica cara Hadrijana 8/A, 31000 Osijek, Croatia; dominik.goman@kemija.unios.hr (D.G.); astankovic@kemija.unios.hr (A.S.); mmkosano@kemija.unios.hr (M.M.-K.)

<sup>3</sup> Department of Organic Chemistry, Faculty of Chemistry and Technology, University of Split, Ruđera Boškovića 35, 21000 Split, Croatia

\* Correspondence: igor@ktf-split.hr (I.J.); sjokic@ptfos.hr (S.J.); Tel.: +385-21-329-436 (I.J.); +385-31-224-333 (S.J.)

**Citation:** Šafranko, S.; Goman, D.; Stanković, A.; Medvidović-Kosanović, M.; Moslavac, T.; Jerković, I.; Jokić, S. An Overview of the Recent Developments in Carbon Quantum Dots—Promising Nanomaterials for Metal Ion Detection and (Bio)Molecule Sensing. *Chemosensors* **2021**, *9*, 138. <https://doi.org/10.3390/chemosensors9060138>

Academic Editors: João Prior and Christos Kokkinos

Received: 28 April 2021

Accepted: 9 June 2021

Published: 11 June 2021

**Publisher's Note:** MDPI stays neutral with regard to jurisdictional claims in published maps and institutional affiliations.



**Copyright:** © 2021 by the authors. Licensee MDPI, Basel, Switzerland. This article is an open access article distributed under the terms and conditions of the Creative Commons Attribution (CC BY) license (<http://creativecommons.org/licenses/by/4.0/>).

**Abstract:** The fluorescent carbon quantum dots (CQDs) represent an emerging subset of carbonaceous nanomaterials, recently becoming a powerful tool for biosensing, bioimaging, and drug and gene delivery. In general, carbon dots are defined as zero-dimensional (0D), spherical-like nanoparticles with <10 nm in size. Their unique chemical, optical, and electronic properties make CQDs versatile materials for a wide spectrum of applications, mainly for the sensing and biomedical purposes. Due to their good biocompatibility, water solubility, and relatively facile modification, these novel materials have attracted tremendous interest in recent years, which is especially important for nanotechnology and nanoscience expertise. The preparation of the biomass-derived CQDs has attracted growing interest recently due to their low-cost, renewable, and green biomass resources, presenting also the variability of possible modification for the enhancement of CQDs' properties. This review is primarily focused on the recent developments in carbon dots and their application in the sensing of different chemical species within the last five years. Furthermore, special emphasis has been made regarding the green approaches for obtaining CQDs and nanomaterial characterization toward better understanding the mechanisms of photoluminescent behavior and sensing performance. In addition, some of the challenges and future outlooks in CQDs research have been briefly outlined.

**Keywords:** carbon quantum dots; green synthesis; ion sensing; biosensing

## 1. Introduction

Carbon-based nanomaterials have recently gained significant research interest due to their extraordinary properties, including thermal stability, mechanical strength, good biocompatibility, and non-toxicity, which opens up a wide range of applications in various research fields [1]. Carbon quantum dots (CQDs) can be classified as zero-dimensional (0D) carbon-based materials with average size less than 10 nm exhibiting excellent photostability and biocompatibility, relatively strong fluorescence properties, and tunable photoluminescence with the possibility of surface functionalization for additional enhancement of these properties [2,3]. The CQDs are commonly described as monodisperse spherical nanoparticles comprised of a carbon core with numerous functional groups

attached to the carbon surface [4,5]. Accidentally discovered in 2004 by Xu et al. [6], fluorescent fragments of single-walled carbon nanotubes (SWNTs) produced during a purification procedure, nowadays known as CQDs, were produced and identified for the first time, while Sun et al. [7] were the first to designate those fluorescent particles as carbon quantum dots.

The presence of oxygen moieties and functional groups on the carbon surface, such as  $-OH$ ,  $-COOH$ , and  $-NH_2$  groups, can impart a high solubility to CQD particles in water, allowing the broader spectrum of potential applications, mainly in the analytical, biomedical, and photoelectronic purposes (Figure 1). Different synthetic methods for the CQDs preparation as well as the involvement of diverse carbon precursors and heteroatom dopants play a key role toward obtaining high quantum yield (QY) fluorescent particles with a great potential for using CQDs as fluorescent probes or biomarkers in cellular imaging [4,8]. Hence, these chemical characteristics, photostability, resistance to photobleaching, and extraordinary optical properties have been extensively studied for applying CQDs in bioimaging, biosensing, and drug and gene delivery purposes [8,9–11].

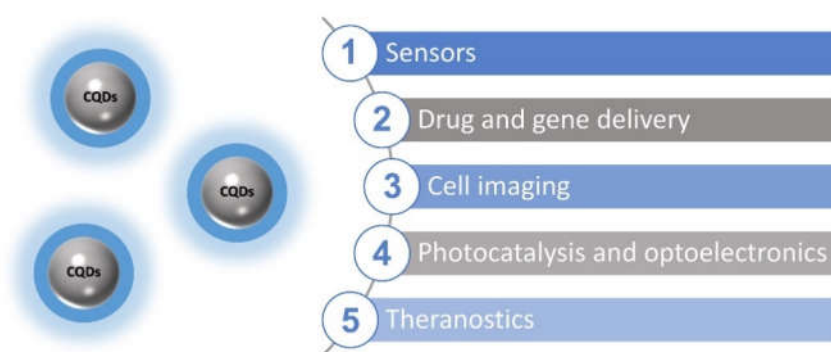


**Figure 1.** Potential applications of CQDs.

Recently, a great deal of effort has been devoted into exploring new and green methods for CQDs preparation with an emphasis on the environmentally friendly approach, simplicity, high QY, uniform size distribution, and large-scale production. It is well-known that the synthesis of transition metal quantum dots (such as cadmium selenide (CdSe), cadmium telluride (CdTe), cadmium sulfide (CdS), etc.) exhibits good performance in the terms of stability and optical characteristics; however high synthetic costs and low biocompatibility has limited their application in biomedicine, more precisely in theranostic purposes [12]. Therefore, biomass has emerged as a potential carbon source and sustainable material for obtaining non-toxic and highly efficient CQDs. These features represent a promising technique for converting biomass or biomass waste into novel material suitable for biomedical and pharmaceutical purposes, as well as in chemical ion and species detection for the purposes of environmental monitoring [13]. Among various possible applications, heavy metal ions and chemical sensing are the most common studied in terms of CQDs research. Some metal ions such as iron ( $Fe^{3+}$ ), zinc ( $Zn^{2+}$ ), and copper ( $Cu^{2+}$ ) elements have an essential role in biological functions and processes; hence, novel, facile, and cost-effective methods of detection are undoubtedly of interest. Among these essential ions, more toxic elements such as mercury ( $Hg^{2+}$ ) and lead ( $Pb^{2+}$ ) could be found accumulated in trace amounts in the human body, hindering normal biological functions by chelation with important biomolecules (enzymes, nucleic acids). However, detection of the present ions is still an interesting research topic even for the environmental sciences and monitoring [14,15]. A development of low-cost, simple, and efficient techniques for the versatile chemical analyte detection is nowadays especially welcomed, and CQDs-based sensors have been extensively studied due to their efficiency, stability, relatively

facile modification toward better selectivity, large specific active area, and superior performance.

Therefore, this review is focused on the carbon quantum dots and their applications in sensing of different molecules and metal ions, which is important for biomedical, pharmaceutical, and environmental purposes, with an emphasis on the research published within the last five years. The emphasis has been also placed on the recent developments in the synthesis as well as potential modifications, doping, functionalization, and characterization of CQDs and biomass-derived CQDs with the aim of properties enhancement, which could provide new insights into the mechanisms and future detection methods of different chemical species with superior performance. Here, their optical and chemical properties, emphasizing the advances and novel green approaches toward obtaining fluorescent nanomaterials with a wide spectrum of applications in sensing, are also discussed in detail. Finally, new perspectives are brought up in order to emphasize the numerous opportunities, as well as the challenges that are still being raised and are critical toward discovering the full potential of these powerful nanomaterials.

## 2. Methods for Preparation of Carbon Quantum Dots

By discovering carbon-nano dots in the last decade, Xu et al. [6] have introduced the novel fluorescent nanomaterials that have been widely used in the various research field such as in chemical sensing [10,12–15], biology [16], nanomedicine [17,18], and photocatalysis [19]. This research group in 2004 isolated novel nanomaterial during the electrophoretic purification process of single-walled carbon nanotubes (SWCNTs) by the arc-discharge technique [6]. In addition, they obtained short, tubular carbon and a mixture of fluorescent carbon nanoparticles derived from SWCNTs, which were observed under 365 nm UV light. Two years later, Sun et al. [7] reported on the preparation procedure and characterization of quantum-sized analogues named as “carbon dots” by laser ablation of carbon target comprised of graphite powder and cement. After post-treatment and surface passivation of the sample by the addition of diamine-terminated oligomeric poly-(ethylene glycol), known as PEG<sub>1500N</sub>, they have observed bright luminescence emission.

In general, synthetic approaches for obtaining CQDs can be classified into two main groups: top-down and bottom-up techniques.

### 2.1. “Top-Down” Approach

The “top-down” technique is based on cutting larger carbon material into nanoparticles, and it includes arc discharge [6], laser ablation [7,15], chemical oxidation [20–23], and electrochemical synthesis [24–26]. Chemical oxidation is classified as one of the “top-down” approaches for obtaining CQDs using strong oxidants, such as nitric acid, sulfuric acid, and hydrogen peroxide (H<sub>2</sub>O<sub>2</sub>). This approach is considered facile and efficient, providing the possibility of large-scale production of CQDs [26]. Ray et al. [22] have synthesized fluorescent nanoparticles by mixing 5 M nitric acid and carbon soot collected from a burning candle, which was followed by reflux at 100 °C for 6 h, 12 h, and 18 h. As expected, carbon soot was completely insoluble in water because of its hydrophobic nature; however, after chemical treatment with nitric acid, the particle size reduced and water-soluble particle were observed. The study also reported that various fractions of CQDs were isolated obtaining different-sized nanoparticles, while it was determined that the smaller particles exhibited better photoluminescence efficiency with the potential application in cellular imaging. The major observations were based on the chemical changes on the surface of the particles, as it was found that the refluxing step made 2-fold modifications, including nitrogen and oxygen incorporation. However, the importance of improving the low yield of the final product was also highlighted, as the significant amount of insoluble carbon soot residue has remained. Moreover, Chen et al. [27] presented a novel approach toward obtaining polyethyleneimine (PEI)-capped carbon dots (PEI-CQDs), which exhibited strong fluorescence emission  $\lambda_{EM} = 446$  nm when excited at  $\lambda_{EX} = 365$  nm. The homogeneous mixture of citric acid and PEI as starting materials was refluxed and

heated up to 120 °C for 2 h. Except for the presence of the oxygen-functional groups, nitrogen was also detected in the samples due to the abundance of amino groups in the PEI precursor. The prepared N-doped CQDs demonstrated potential application in Cu<sup>2+</sup> sensing. The chemical oxidation has shown a lot of advantages in efficient CQDs preparation and functionalization; however, except for low yields, another great challenge represents the establishment of an efficient purification protocol for obtaining non-toxic material for potential biomedical and biological applications. These steps usually include the removal of strong acids, dialysis protocols, and pH adjustments that could have a negative impact on the in vitro or in vivo experiments [25].

Moreover, the electrochemical synthesis of CQDs has gained increasing attention recently due to its simplicity and mild operating conditions, as it can be carried out under normal temperatures and pressures [28]. This synthetic method is also recognized as a suitable method for tuning particle size, directly affecting the photoluminescence properties [25,28]. In 2016, Liu et al. [29] reported the preparation of CQDs from a facile electrochemical oxidation of a graphite electrode in alkaline alcohols. The obtained CQDs showed high crystallinity and biocompatibility, particles had an average diameter of ( $d = 4.0 \pm 0.2$ ) nm and were used for cellular imaging as well for Fe<sup>3+</sup> detection with a broad linear range from 10 to 200 μM and limit of detection of 1.8 μM. The as-prepared CQDs were colorless and were stored at 4 °C; however, during exposure at room temperature, the CQDs dispersion turned to a bright yellow color. This led to an interesting observation that changes in sample color could be related to the changes of surface states due to the oxidation. Moreover, Hou et al. [30] also reported on the synthesis of water-soluble and blue-emission CQDs by electrochemical carbonization using sodium citrate and urea as starting materials. The obtained samples demonstrated a high quantum yield of 11.9% and low limit detection of 3.3 nM, and they were used as an electrochemical sensing probe for the determination of Hg<sup>2+</sup> ions in model systems as well as in the real water samples. Although the electrochemical procedures showed a lot of advantages in efficiently obtaining CQDs with high yield and low-cost production, the tedious purification of the final products could be considered the main disadvantage of this method [31,32].

## 2.2. “Bottom–Up” Approach

The higher flexibility of the “bottom–up” approach by the means of the selection of chemical precursors and applying optimal operating conditions makes “bottom–up” methods more favorable techniques for obtaining different CQDs. Thermal/combustion techniques are the most commonly reported synthetic routes for CQDs preparation due to their simplicity, better variability of using different carbon sources, surface functionalization, environmental friendliness, and lower costs of synthesis [5,12,33]. Another important advantage of the “bottom–up” approach is better control over the particle size, morphology, and chemical composition. In general, this approach generates CQDs from different precursors (smaller molecules or heterogeneous sources) by thermal treatment [33,34]. Very often, this includes rigorous thermal treatment at high temperatures as well as sample treatment with concentrated acids and bases. However, the possibility of using different chemical precursors of different carbon origin gives a rise to the variability in CQDs properties; therefore, it widens the spectrum of possible applications in different research fields. These particles could be obtained by employing different “bottom–up” approaches including hydrothermal/solvothermal treatment [14,15,35], carbonization [25,36,37], microwave-assisted synthesis [38,39], thermal decomposition, and pyrolysis [40,41]. It is well known that surface functionalization and heteroatom doping of CQDs could enhance properties of obtained nanomaterials, mainly electronic, optical, and chemical properties, and it could also affect the selectivity and affinity toward ion and (bio)molecule detection and sensing. Usually, the most commonly used precursors for obtaining CQDs using “bottom–up” approaches are citric acid [42–44], glucose [45], amino acids [46,47], and natural products. The addition of the different molecules with distinct functional groups attached onto the CQDs surface could enhance quantum yield (QY), optical

properties in general, and also surface reactivity. The most commonly used dopant in hydrothermal synthesis is undoubtedly nitrogen (N doping), while there are few works reporting the preparation of sulfur (S-doped) [48], and phosphorus (P-doped) [49] CQDs. Recently, Kalaiyarasan et al. [49] prepared P-doped CQDs by employing a hydrothermal approach using an aqueous mixture of trisodium citrate and phosphoric acid and heated at different temperatures by increasing the temperature rate (3 °C/min) at different time intervals. The optimal conditions toward maximizing QY were determined as 140 °C and 12 h with an obtained quantum yield of QY = 16.1%. The interesting observation has been made regarding the added concentration of phosphoric acid. At higher phosphorus content,  $\lambda_{EX}$ -dependent fluorescence nature has been observed, most probably as a consequence of the reduced value of the doped phosphorus/oxygen ratio and increasing the oxygen content on the CQDs surface. The degree of P doping of CQDs was proportional to the added content of phosphorus. The obtained P-CQDs were used for the sensing and detection of Fe<sup>3+</sup> ions through formation of the fluorescence-inactive P-CQDs-Fe<sup>3+</sup> chelation complex. Moreover, the synthesis of S-doped CQDs was reported by Yang et al. [50] for the detection of Sudan I, synthetic diazo-conjugate dye with potential cancerogenic and mutagenic effects, which still can be found illegally as a food additive in ketchup. The pre-hydrolyzed lignin was used as a precursor and sulfuric acid was used as a dopant, and mixture was exposed to the hydrothermal synthesis at temperature of 220 °C for 11 h. The obtained S-doped CQDs showed good quantum yield of QY = 13.5%, while elemental analysis of samples showed the presence of sulfur-containing groups on the CQDs surface. The nanoparticles showed good sensitivity and selectivity toward Sudan I with a calculated LOD = 0.12  $\mu$ M by the fluorescence quenching mechanism. The sample also exhibited good performance in acidic environment (pH ranged from 0 to 5.0) showing great potential as a low-cost and fast assay toward Sudan I detection. All the discussed synthetic approaches with corresponding advantages and disadvantages are presented in Table 1.

**Table 1.** Summary of advantages and disadvantages of CQDs synthetic methods.

| Method                              | Advantages (Pros)                                | Disadvantages (Cons)                 | References |
|-------------------------------------|--|--------------------------------------|------------|
| <b>“Top-down” approach</b>          |  |                                      |            |
| Arc discharge                       | -  | -                                    | [7,22,51]  |
| Laser ablation                      | - Simple procedures                              | - Difficult to control particle size |            |
| Chemical oxidation                  | - Cheap raw material                             | - Expensive equipment                |            |
| Electrochemical oxidation           | - Mass production                                | - Long processing time               |            |
| <b>“Bottom-up” approach</b>         |  |                                      |            |
| Hydrothermal/solvothermal treatment | - Good control of particle size and morphology   | -                                    | [33,51]    |
| Carbonization                       | -  | - Often include complex procedure    |            |
| Microwave-assisted synthesis        | - Low-cost                                       | - Possible aggregation               |            |
| Thermal decomposition and pyrolysis | - Facile synthesis and surface functionalization | -                                    |            |

### 2.3. CQDs Preparation from Natural Sources

Previously, inorganic quantum dots have been widely studied due to their outstanding photostability, electronic, and catalytic activity. These properties have enabled the application of these semiconductor materials in different research areas, from basic and applied research to biomedical applications [52]. The greatest limitation for possible metal quantum dots application in biological and environmental research is the low biocompatibility due to the presence of toxic and heavy metal content, which are mostly comprised of cadmium (CdTe, CdS, CdSe, etc.) [15]. Therefore, CQDs have emerged as promising and biocompatible fluorescent nanomaterials as a decent substitution for cellular imaging and sensing. The biocompatibility and low cytotoxicity are of great importance for the

biomedical and pharmaceutical research, and nowadays, many studies have been reported using CQDs for the purposes of bioimaging, drug delivery, or for theranostic purposes. An overview of the different CQDs prepared from various sources of biomass, their properties, and applications are shown in Table 2. Recently, CQDs derived from biomass have shown superior performance in sensing and imaging applications. A biomass can be considered as a good source of carbon, and using natural products for the preparation of CQDs often enables simple doping by the heteroatoms naturally found in biomass products [2]. The preparation of CQDs from low-value biomass, such as by-products and wastes, could be an example of efficient conversion of low-value products into valuable materials with a wide spectrum of possible applications. The literature data have shown that biomass has been widely used for the synthesis of efficient CQDs such as tomato [53,54], potato [55], expired milk [56] (Figure 2), and different plant material (Table 2); however, recently, the preparation of CQDs from waste of different origin (agricultural, industrial, domestic) covers more of this research topic and focuses also on the important concerns regarding the environmental impact and efficient waste management.

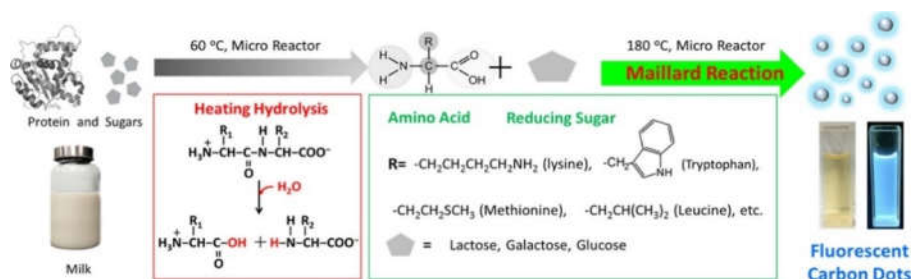


**Figure 2.** Schematic illustration of the step-by-step preparation of N-CQDs using expired milk as a source of carbon and nitrogen, showing also intermediate products of the hydrolysis of proteins and Maillard reactions [56].

**Table 2.** CQDs prepared from the biomass and waste carbon sources and their properties and applications.

| Raw Material           | Synthesis                                     | Modification            | QY   | Application  | Reference |
|------------------------|---|-------------------------|--|--|-----------|
| <b>Biomass</b>         |   |                         |  |  |           |
| Glucose                | Continuous hydrothermal flow synthesis (CHFS) | ND <sup>1</sup>         | 0.3%   | Detection of Cr <sup>6+</sup> and Fe <sup>2+</sup> ions        | [45]      |
| Rice residue           | Hydrothermal                                  | Lysine                  | 23.48%   | Detection of Fe <sup>3+</sup> ions and tetracycline–antibiotic | [46]      |
| Cherry tomato          | Hydrothermal                                  | ND <sup>1</sup>         | 9.7%   | Detection of trifluralin–herbicide                             | [53]      |
| Fresh tomato           | Microwave-assisted synthesis                  | EDA <sup>2</sup> , urea | 1.77% (raw material), 7.9% for EDA, and 8.5% for urea (modified) | Vanillin detection   | [54]      |
| Potato starch          | Acid-assisted ultrasonic route                | Acid oxidation          | 10.0% (standard: Rhodamine B)                                    | Detection of Zn <sup>2+</sup> ions                             | [55]      |
| Expired milk           | Subcritical water synthesis                   | ND <sup>1</sup>         | 8.64%  | Detection of Fe <sup>3+</sup> ions                             | [56]      |
| Citrus lemon juice     | Hydrothermal                                  | EDA <sup>2</sup>        | 31.0%  | Detection of Hg <sup>2+</sup> ions                             | [57]      |
| <i>Rosa roxburghii</i> | Hydrothermal                                  | ND <sup>1</sup>         | 24.8%  | Detection of <i>o</i> -nitrophenol                             | [58]      |
| Carrot                 | Hydrothermal                                  | PEI <sup>3</sup>        | 11.5%  | Detection of S <sup>2-</sup> ions                              | [59]      |
| Spinach                | Hydrothermal                                  | ND <sup>1</sup>         | 53.0%  | Detection of 2-nitrophenol (2-NP) and 4-nitrophenol (4-NP)     | [60]      |

|  |                                  |  |  |  |      |
|--|----------------------------------|--|--|--|------|
| Mixture of lemon and onion juice   | Microwave-assisted carbonization | NH <sub>4</sub> OH   | 23.6%  | Riboflavin   | [61] |
| Cranberry beans  | Hydrothermal                     | ND <sup>1</sup>  | 10.85%   | Detection of Fe <sup>3+</sup> ions                                   | [62] |
| Onion extract  | Hydrothermal                     | EDA <sup>2</sup>   | 6.21%  | Detection of Zn <sup>2+</sup> ions in blood plasma                   | [63] |
| <b>Waste</b>   |                                  |  |  |  |      |
| Orange peel (OP), ginkgo biloba leaves (GB), paulownia leaves (PL), and magnolia flower (MF) | Hydrothermal                     | ND <sup>1</sup>  | 4.29% (OP-CQDs), 7.72% (GB-CQDs), 4.74% (PL-CQDs), 8.13% (MF-CQDs) | Detection of Fe <sup>3+</sup> ions                                   | [64] |
| Lemon peel   | Hydrothermal                     | Acid oxidation (0.1 M H <sub>2</sub> SO <sub>4</sub> /TiO <sub>2</sub> ) | 14.0%  | Detection of Cr <sup>6+</sup>  | [65] |
|  | Hydrothermal                     | ND <sup>1</sup>  | 11.0%  | Detection of carmine in beverages (E120)                             | [66] |
| Mango peel   | Hydrothermal                     | Toluene, APTES <sup>4</sup>  | ND   | Detection of mesotrione-herbicide                                    | [67] |
| Onion waste  | Carbonization                    | EDA <sup>2</sup>   | 28.0%  | Detection of Fe <sup>3+</sup> ions                                   | [68] |
| Pineapple peel   | Hydrothermal                     | Ethanol  | 42.0%  | Detection of Hg <sup>2+</sup> ions                                   | [69] |
| Fuel waste   | Chemical oxidation               | HNO <sub>3</sub>   | 3.0%   | Detection of picric acid, Cu <sup>2+</sup> and Fe <sup>3+</sup> ions | [70] |
| Taro peel  | Carbonization                    | H <sub>2</sub> O <sub>2</sub> ; Eu <sup>3+</sup>                         | 13.80%   | Detection of F <sup>-</sup> ions                                     | [71] |

<sup>1</sup> ND—no data presented, <sup>2</sup> EDA—ethylenediamine, <sup>3</sup> PEI—polyethylenimine, <sup>4</sup> APTES—(3-Aminopropyl)triethoxysilane.

It is interesting that biomass-derived CQDs can be used to detect metal ions and some molecules, and some selected examples are shown in Table 2. The preparation of CQDs and N-doped CQDs from fresh tomato has been reported by Liu et al. [54] for the application of vanillin detection and bioimaging of plant pathogenic fungi. The CQDs have been synthesized by microwave-assisted pyrolysis of the fresh tomato as a carbon source (P-CQDs), while N doping was carried out using ethylenediamine (EDA; E-CQDs) and urea (U-CQDs). The calculated quantum yield has shown that pristine, non-modified P-CQDs exhibited a low quantum yield of QY = 1.77%, and for N-doped CQDs, E-CQDs exhibited a low quantum yield of QY = 7.9% and U-CQDs exhibited a low quantum yield of QY = 8.5%. As it can be observed, the significant increase in QY was probably caused by the N doping and by an increase in nitrogen content. The N-dopants, EDA and urea containing amino groups, acted as nucleophiles, and they most likely affected the particle size, structural characteristics, and chemistry surface. The prepared U-CQDs have been used for the vanillin detection in sugar, which is a phenolic aldehyde and dominant aroma in vanilla bean. The fluorescence intensity of U-CQDs in the presence of vanillin has been investigated within a concentration range from 0 to 200 µM, while good linear range was obtained from 3.0 to 55.0 µM. The method was evaluated by testing the detection of vanillin in commercial sugar, and recoveries ranged from 96.6 to 105.9% with an LOD of 24.9 mg kg<sup>-1</sup>. As previously mentioned, surface modification (functionalization and passivation) and doping could enhance the beneficial properties of CQDs such as QY, optical, and chemical characteristics. Nitrogen doping of CQDs has been widely applied for the efficient properties enhancement of CQDs [72]. An interesting example of CQDs preparation from waste material was presented by Boruah et al. [71] using taro peel as a carbon source. The CQDs were prepared by H<sub>2</sub>O<sub>2</sub> chemical treatment of taro peel, followed by ultrasonication for 3–4 h. The obtained nanoparticles of size 8–12 nm, containing more oxygen functional groups on the surface and with high QY = 26.20%, were estimated to

be a promising nanoprobe for the fluoride ( $F^-$ ) ion detection in water samples. Prior to the detection of the fluorides in water, the nanoprobe comprised of the complex of CQDs and  $Eu^{3+}$  was prepared for the fluorescence quenching enhancement. It has been reported that  $Eu^{3+}$  could be considered as hard acid according to the HSAB theory, having great affinity for the hard base such as  $F^-$  ion in water. It is also suggested that  $Eu^{3+}$  binds to the  $-COOH$  groups on the CQDs surface, which was confirmed by X-ray photoelectron spectroscopy (XPS).

### 3. Material Characterization

In general, the properties of each individual CQD strongly depend on the applied synthetic techniques as well as on the selection of the carbon precursors, surface passivation and functionalization, heteroatom doping, and applied temperature and exposure time [73]. These factors directly influence the efficiency of the prepared materials as well as applicability in different scientific and research fields, such as electronics, environmental, and biomedical analysis. The applicability of the prepared CQDs is affected by the biocompatibility, solubility in different media, quantum yield (QY), and wavelengths of the emission and blue- and red-shifts of the absorption spectra [74,75].

#### 3.1. Structural and Chemical Properties

From the chemical and structural aspects, CQDs are composed of the carbon core decorated with different functional groups on the surface, which are mainly present as carboxyl, hydroxyl, carbonyl, and amide moieties. The structural characteristics of CQDs can differ; however, there are mostly referred to as carbon materials with a low degree of crystallinity containing disordered domains. Hence, a disorder in the CQDs structure could appear due to the presence of the  $sp^2/sp^3$  variable ratio [75,76]. The phenomenon could be detected and observed by X-ray diffraction (XRD) patterns. In the study by Edison et al. [76] the preparation of N-doped CQDs was reported. The N-CQDs were prepared by microwave-assisted synthesis of the ascorbic acid and  $\beta$ -alanine mixture, and structural analysis has been performed by XRD, Raman spectroscopy, and Fourier-transform infrared spectroscopy (FTIR). Raman spectroscopy is also considered as one of the most useful techniques for the structural characterization of CQDs and carbon-based nanomaterials in general. The FTIR analysis is useful to gain insight into the basic chemical composition based on the attached functional groups. The XRD pattern has shown two broader diffraction peaks approximately at  $2\theta = 23.7^\circ$  and  $2\theta = 42^\circ$ , which correspond to disordered carbon atoms with a high degree of (002) and (100) planes for the hexagonal graphite structure (N-CQDs). In addition,  $d$ -spacing has been calculated according to the Bragg's equation, and it was determined to be  $d = 0.37$  nm for (002) and  $d = 0.21$  nm for the (100) peak. The broader peaks are contributed by the smaller size of N-CQDs [76]. The Raman spectrum showed two bands at  $1365\text{ cm}^{-1}$  and  $1595\text{ cm}^{-1}$ , corresponding to  $sp^2$ -hybridized carbon (G band) and  $sp^3$  present defects (D band) in the prepared N-CQDs, respectively. Generally, the D band is related to the defects in the graphite lattice presenting possible disorders in the structure (presence of  $sp^3$ -hybridized carbon). The G band is related to the presence of the  $sp^2$ -hybridized carbon network. The parameter ( $I_D/I_G$ ) represents the intensity ratio of the D and G bands and could indicate possible defects in the CQDs structure arising from the oxidation process or by the presence of the hetero groups on the surface [76]. In this literature, Edison et al. [76] reported a CQDs structure with fewer defects, as the determined ( $I_D/I_G$ ) ratio was  $<1$ ; more precisely, the ( $I_D/I_G$ ) ratio was 0.77. Furthermore, Jing et al. [77] also characterized CQDs derived from carbonized glucose with remaining hydrochar, and the XRD pattern showed two broad peaks at  $2\theta = 22^\circ$  attributed to the amorphous nature of the obtained nanoparticles and  $2\theta = 44^\circ$  revealing the presence of graphitic carbon. The FTIR analysis showed the presence of hydroxyl and carboxyl groups, and oxygen was present in hydroxyl, carboxyl, carbonyl, and epoxy/ether, which was confirmed by corresponding bands at  $3000\text{--}3715\text{ cm}^{-1}$ ,  $1705\text{ cm}^{-1}$ , and around  $1000\text{--}1100\text{ cm}^{-1}$ . In addition, the FTIR technique could confirm the presence

of attached amine groups by the presence of a band at around 1600–1500  $\text{cm}^{-1}$ . Techniques such as X-ray photoelectron spectroscopy (XPS) are very useful for the elemental analysis of the synthesized sample, with the possibility of the oxygen quantification present on the CQDs surface in the form of carbon–oxygen bonding, as well as the quantification of heteroatoms such as sulfur, nitrogen, phosphorus, boron, etc. In the study by Su et al. [56], nitrogen-doped carbon quantum dots (N-CQDs) were fabricated by using expired milk as a carbon and nitrogen precursor in a subcritical water reactor. Through the reactions of protein denaturation and Maillard reactions, N-CQDs were obtained with QY = 8.64% exhibiting also an excitation wavelength-dependent emission in the wavelength range of  $\lambda_{\text{EM}} = 400\text{--}550$  nm. The XPS full survey spectrum of N-CQDs demonstrated three peaks C 1s (285 eV), N 1s (400 eV), and O 1s (532 eV), indicating the presence of carbon, oxygen, and nitrogen in the composition of N-CQDs. The high-resolution spectra demonstrated that the C 1s band can be deconvoluted into four peaks at 284.7 eV, 286.1 eV, 287.6 eV, and 288.7 eV, corresponding to the C 1s states in C–C/C=C, C–N/C–O, C=O, and COOH, respectively. Moreover, the N 1s spectrum exhibited two peaks at 399.6 and 401.2 eV, corresponding to pyrrolic N and graphite N. The O 1s band showed two peaks at 531.3 and 532.4 eV for C=O and C–O, respectively. In addition, Kalaiyarasan et al. [49] reported the hydrothermal preparation of P-CQDs using trisodium citrate and phosphoric acid with obtained QY = 16.1%. A successful P doping was confirmed with the XPS technique with increasing phosphorus concentration, leading also to the surface passivation with phosphorus moieties. The high-resolution P 2p spectra of P-CQDs have been deconvoluted into two peaks at 132.1 eV and 133.1 eV by the Gaussian function, which can be assigned to P–C (5.70%) and P–O (3.17%) groups. The C 1s spectrum can be deconvoluted into three peaks at 284.1 eV, 285.4 eV, and 288.4 eV by the Gaussian function that can be assigned to aromatic carbon (C–C/C=C, 18.89%), C–O/C–P (7.35%), and C=O (2.42%). However, the carboxylic acid functional moiety in the C 1s spectrum was not observed. The Gaussian function was also used to deconvolute the O 1s spectrum into three peaks at 531.0 eV, 532.4 eV, and 536.0 eV, which can be ascribed to C=O (16.76%), P=O (44.56%), and H<sub>2</sub>O (1.13%) groups. As it can be observed, the amounts of carbon, oxygen, and phosphorus moieties were detected in prepared P-CQDs.

When describing CQDs, the scientists usually define CQDs as nanoparticles of diameter approximately of 10 nm, and this is definitely reported in different literature employing transmission electron microscopy (TEM) [53–55]. Another common characteristic of the CQDs is their monodisperse and relatively narrow size distribution, with spherical or quasi-spherical morphology and particle shape [11,75,78]. Hence, monodispersity and size distribution can be evaluated by both dynamic light scattering (DLS) and TEM techniques, while the fine-structure observation and morphology of CQDs could be examined by high-resolution TEM (HRTEM) [79]. The fabrication of N-CQDs using onion waste as a carbon and nitrogen precursor was reported by Bandi et al. [68]. The nanoparticles were well-dispersed with an average size diameter of 15 nm, which was confirmed both by TEM (average determined size about 15 nm) and DLS analysis (average determined size within the range 7–25 nm). However, more detailed insight into the crystalline nature was provided by HRTEM measurements, and the results indicated the crystalline nature of prepared N-CQDs with a lattice parameter of 0.21 nm, which was probably attributed to the  $\text{sp}^2$  (1120) graphitic crystal phase of graphene. The pH stability and pH vs. fluorescence emission intensities could vary depending on the used precursors and applied method of synthesis. In the literature, it is reported that some biomass-derived CQDs could be used as pH sensors due to their ability to change fluorescence emission intensity or fluorescence lifetime by varying the pH range from extreme acidic to extreme alkaline [72,80]. This could be attributed to the presence of the carboxyl and hydroxyl groups on the surface, and due to the protonation and deprotonation under different pH conditions, the electrostatic charge also changes [72].

Indeed, Huang et al. [80] have reported the preparation of N-CQDs using citric acid and urea in dimethylformamide (DMF) by a solvothermal procedure at 160 °C for 6 h. The

obtained pH-sensitive CQDs were employed for intracellular pH sensing with fluorescence lifetime imaging microscopy (FLIM). It was observed that the fluorescence lifetime of the N-CQDs solutions with different pH values (pH = 2.6–8.6) increased linearly with the increase of pH value. In addition, the fluorescence decay time increased against the pH values of the buffer from 3.2 to 8.3 in the pH buffer-treated cells. It was concluded that the different functional groups attached onto the surface of CQDs were changing depending on the pH microenvironments, which led to the changes of the fluorescence lifetime values. This study showed a potential use of pH-sensitive N-CQDs in intracellular pH sensing in complex biological environments. In addition, by using strong and concentrated acids, useful surface defects and oxygen-functional moieties (hydroxyl, carboxyl, carbonyl) could be generated, which directly influence the reactivity and water solubility of the prepared particles [72,74].

### 3.2. Optical Properties

In general, the characteristic optical absorption spectrum of CQDs observed in the UV region is comprised of two peaks, with a maximum absorption peak at around 260–270 nm corresponding to the  $\pi$ - $\pi^*$  transition (HOMO-LUMO) of the C=C bonding of the  $sp^2$ -hybridized C-domains. The absorption peaks at around 300–330 nm are assigned to the  $n$ - $\pi^*$  transition of the C=O bonding. The presence of the extending tail across the visible region is mostly related to the nanoparticle functionalization [73]. The most important feature of the CQDs is their photoluminescence, allowing their application in bioimaging, biosensing, and the detection of different chemical species in general. For bioanalytical purposes, one of the important factors is QY. The QY related to the CQDs is one of the essential keys toward better performance in bioimaging and biosensing [75]. Lower QY could be considered as one of the main limiting factors for the application in biomedical analysis, as it directly affects the sensitivity and imaging resolution, while the lower sensitivity of the sensor could be considered as a limiting factor in efficient analyte sensing [75,78]. Hence, many efforts have been recently devoted toward the efficient preparation of CQDs exhibiting high quantum yield  $QY \geq 20\%$ .

It is well known that pristine CQDs without any modification exhibit lower quantum yield, and surface passivation or functionalization has been used to improve optical properties, mainly fluorescence emission intensity. If CQDs are considered as carbonaceous materials with  $sp^2$  and  $sp^3$  domains, then on a micro level, it is suggested that CQDs are accompanied with the defects of a non-perfect  $sp^2$  domain, creating energy gaps that impart the photoluminescence features of CQDs [81]. Although the precise explanation of the photoluminescence is still disputable, there are three possible explanations that could elucidate the mechanism through (1) the quantum confinement due to the conjugated  $\pi$ -domains of the carbon core, (2) surface states due to the presence of functional groups attached on the carbon backbone, and (3) a molecular state, which is explained by the photoluminescence originating from free and/or bonded fluorescent molecules [73].

The surface passivation refers to the treatment of CQDs using polymers and organic molecules stabilizing surface energy traps that participate in fluorescence emission. In addition, capping the pristine CQDs with a thin protection layer of long-chain agents shields the prepared CQDs from impurities adhesion, which could have a negative impact on the particle stability and optical properties [74]. As already mentioned, introducing heteroatoms to the CQDs could also improve different properties as well as the electric, optical, and chemical features of CQDs. Due to its similar atomic size and higher electronegativity compared to a carbon atom, having also five electrons in its outer shell, nitrogen has been widely used for the carbon materials doping [72,76]. However, sulfur and phosphorus are also used for the heteroatom doping of CQDs due to their atomic characteristics, as both elements have a larger atomic radius and could easily create disorders within the carbon backbone. Some of these procedures could also induce the red-shift fluorescence, or the emission shift toward longer wavelengths, which is mainly caused by introducing electron-withdrawing groups on the CQDs surface. It is reported that red-shift emission is

more convenient for the analysis and sensing as UV radiation could be harmful for the biological systems, and shifting the excitation toward longer wavelengths could reduce this risk [2].

#### 4. Sensing Mechanisms

Although there are several mechanisms responsible for the changes in the fluorescence properties in CQDs, this phenomenon is based on the CQDs and fluorophore interaction, which quenches or enhances the fluorescence intensity [82]. There are a few mechanisms reported that cause a quenching or enhancing effect on the fluorescence: static quenching, the dynamic quenching mechanism, photoinduced electron transfer (PET), energy transfer (ET), and the inner filter effect (IFE). The energy transfer could be further classified into three different mechanisms as Förster (fluorescence) resonance energy transfer (FRET), Dexter energy transfer (DET), and surface energy transfer (SET) [83]. The mechanism of static quenching could be explained as that which occurs when a non-fluorescent ground-state complex is formed due to the interaction of the quencher and CQDs, while the dynamic quenching mechanism could occur by the return of the excited states to the ground state as a consequence of the CQDs and quencher collision due to the charge or energy transfer [82,83]. The FRET mechanism includes the transfer of non-radiative energy between a luminescent donor (first fluorophore; CQDs) and an energy acceptor (second fluorophore; quencher) within a close range of approximately 10 to 100 Å [83,84]. The FRET mechanism occurs between CQDs in the excited state and a quencher in the ground state, and the emission spectrum of CQDs overlaps with the absorption spectrum of the quencher. Hence, it could be suggested that the efficiency of the mechanism is dependent on the spectral overlapping between CQDs and the quencher, the spatial distance between the quencher and CQDs, and the fluorescence QY. It is also reported that during the FRET, the fluorescence lifetime would decrease [83]. Furthermore, the DET process occurs through redox reactions and requires the match between redox potential of donor and acceptor [83], while the SET mechanism is a novel approach including a metal surface (metal nanoparticle) and molecular (organic) dipole.

#### 5. Photoluminescent Sensing of Metal Ions

In general, for the detection of individual chemical analytes, the development of a highly sensitive, selective, low-cost, and practical analytical method and sensor is desirable. Conventional analytical methods for the detection of different metal ions mostly include bulky instruments as well as special and time-consuming sample preparation, and these methods are not always convenient. Therefore, the development of more practical and less expensive methods is particularly welcomed in the analytical practice. These novel techniques in analyte sensing mostly include electrochemical methods, fluorescence methods, chemiluminescence methods, quartz crystal microbalance, etc. Among those mentioned, fluorescence methods are recognized for their precision and accuracy as well as higher selectivity and sensitivity for the target compound and also for the simplicity of performing measurements. The key factor in the development of a fluorescence sensor is the design of a suitable fluorophore with a good sensing performance [82]. The performance is affected by fluorescence lifetime, fluorescence QY, the width and the shape of the emission bands and maximum, Stokes shifts, etc. Another important factor is the type of the prepared CQDs and the presence of functional groups on the surface, which could interact with different chemical species. For the sensing purposes, CQDs are mostly used for the detection of different metal ions, especially for the sensing of heavy metals. Heavy metals are ubiquitously distributed in the environment, and their role is most commonly presented as contaminants, but based on their toxicity, heavy metals are classified into two groups: essential and nonessential heavy metals [85]. Heavy metals such as Hg, Pb, As, and Cd are classified as extremely toxic and mutagenic elements for human health, and these elements are nonessential for plants and animals, presenting also extreme danger for environmental accumulation. Elements such as Zn, Cr, and Cu are classified as

essential micronutrients at lower concentration, presenting a potential risk with the increase in concentration [82]. Hence, efficient sensing and detection of different ions, mostly heavy metals, is of a great importance for environmental monitoring and health risk assessment.

### 5.1. Ferric ( $Fe^{3+}$ ) Ions Detection

According to the literature, ferric ions have been the most commonly detected ions using CQDs as a fluorescent nanoprobe [2]. The main reason of this common phenomenon is due to the presence of the amino, carboxyl, and hydroxyl functional groups on the surface, which could interact with the  $Fe^{3+}$  easily and effectively, resulting in fluorescence quenching. It is well known that ferric ions exist in the biological systems and in the environment, but the excessive exposure to these ions could induce severe disease, such as kidney failure, liver damage, etc. [86]. Therefore, efficient methods for the monitoring of  $Fe^{3+}$  in biofluids and the environment could be useful for analytical practice. The novel CQDs-based sensors for the detection of  $Fe^{3+}$  ions are listed in Table 3. A report by Issa et al. [86] includes preparation of the N-CQDs from carboxymethylcellulose (CMC) and polyethyleneimine (LPEI) by hydrothermal synthesis at 260 °C for 2 h (Figure 3).

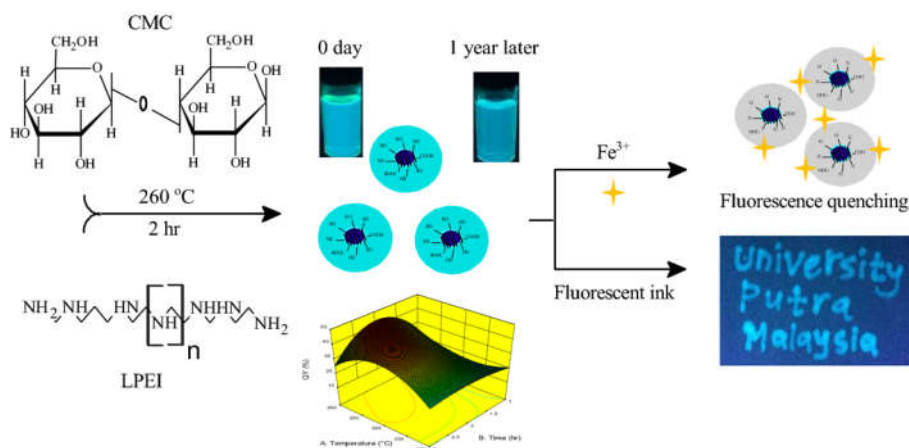


**Figure 3.** Schematic illustration of the synthesis of N-CQDs using CMC and LPEI as precursors; their application in  $Fe^{3+}$  sensing and as fluorescent ink [86].

The product of N-CQDs was purified by a filtration and dialysis (1kDa) procedure. Interestingly, process optimization was performed using response surface methodology (RSM), which is a mathematical tool using independent variables to optimize response, which is in this case photoluminescence (PL) QY. Each variable was used including synthesis temperature ( $X_1$ ), time exposure ( $X_2$ ), and LPEI weight ( $X_3$ ) to optimize the process regarding QY through the face-centered central composite design (CCD) through 18 experiments. Finally, quadratic model was selected for the modeling, and the results have shown the significant influence of the interaction of the applied temperature ( $X_1$ ) and time exposure ( $X_2$ ) on the QY. It was concluded that variables have a synergistic influence on the QY. The optimum conditions for obtaining QY of 43.92% were predicted by the model and it was as follows: temperature of 260 °C, time exposure of 2 h, and LPEI weight of 1%. The mode was experimentally evaluated, and the obtained QY is determined to be 44%, which is very closely to the predicted value. The prepared particles were further used for the detection of the  $Fe^{3+}$  in the acidic environment at pH = 3. Typically,  $Fe^{3+}$  ions using CQDs were analyzed under natural conditions, and mostly, the PL intensity of N-CQDs is unstable under these conditions. In the study by Issa et al. [86], the detection of  $Fe^{3+}$  ions in acidic environment was enabled by the presence of  $-OH$ ,  $-COO^-$ , and  $-NH$  functional groups around the N-CQDs edge, and these groups can act as a bridge to bind the nanoprobe with any surrounding analytes. The developed method showed a wide linear range

from 1 to 400  $\mu\text{M}$ , with a coefficient of determination of  $R^2 = 0.9933$ . The limit of detection (LOD) was calculated to be 0.14  $\mu\text{M}$ . The possible mechanism is explained through the higher affinity of the  $\text{Fe}^{3+}$  ions for the oxygen/nitrogen electron donors, resulting in the coordination and covalent bonds formation between the atoms. The new formed bonds resulted in the migration of the excited electrons to the vacant  $d$ -orbitals of  $\text{Fe}^{3+}$ , leading to non-radiative recombination of the excitons (e-h) causing the PL quenching [86]. The significance in the  $\text{Fe}^{3+}$  and in many other ions sensing at low pH was also emphasized by Yang et al. [87]. Due to the presence of the metal contaminants in the form of suspended solids in aquatic environments, acidic treatments of the samples are required in order to determine the total soluble metal content and to improve the selectivity and sensitivity of each specific sensor. In a previous study by Yang et al. [87], an acidophilic S-doped CQDs sensor was prepared by the hydrothermal treatment of cellulose fibers, which were previously hydrolyzed by using 64% ( $w/w$ ) sulfuric acid. Hydrothermal treatment was carried out at 200  $^\circ\text{C}$  for 4 h in oven. The primarily aim was the conversion of cellulose fibers into the hydrophilic nanoparticles and also the preparation of CQDs particles by a carbonization procedure. The obtained S-CQDs exhibited strong fluorescence emission with an estimated QY = 32%. The fluorescence response under different pH conditions showed interesting results, as the PL intensity increases as the pH value decreases. This phenomenon could be attributed to the different deprotonation degrees of the S-CQDs at different pH values. The outstanding selectivity and sensitivity of the prepared CQDs-based sensor demonstrated potential application in  $\text{Fe}^{3+}$  detection in acidic environments (pH = 0) with an obtained LOD = 0.96  $\mu\text{M}$ . Another interesting example is the study of the Liu et al. [88] with N-CQDs fabrication from *Fusobacterium nucleatum*, which is an anaerobic Gram-positive oral commensal bacteria that was a single precursor for the hydrothermal synthesis of N-CQDs at 180  $^\circ\text{C}$  for 12 h. The selectivity measurements showed the selective response toward  $\text{Fe}^{3+}$  ions, and a good linear response was obtained within the linear concentration range from 20 to 180  $\mu\text{M}$  with an obtained  $R^2 = 0.9855$ . The estimated LOD was 0.82  $\mu\text{M}$ . The mechanism of the quenching was also investigated, and it was concluded that the main reasons for the fluorescence quenching was ion exchange or energy transfer. Furthermore, the CQDs and  $\text{Fe}^{3+}$  interaction was investigated for the application of CQDs as an intracellular  $\text{Fe}^{3+}$  biosensor. As biocompatible nanoparticles, the incubation and analysis of the prepared N-CQDs and  $\text{Fe}^{3+}$  suggested that fluorescence was quenched by the presence of  $\text{Fe}^{3+}$  ions in living cells. This also suggested the potential application of the prepared N-CQDs for in vitro and possible in vivo bioimaging and biosensing.

**Table 3.** Summary of the literature reporting methods of  $\text{Fe}^{3+}$  ions detection of the past five years (2016–2021).

| CQDs-Based Sensor                             | Type of CQDs      | QY (%)          | $\lambda_{\text{EX}}/\lambda_{\text{EMmax}}$ | Linear Range             | LOD                  | Reference |
|---|-------------------|-----------------|--|--------------------------|----------------------|-----------|
| CQDs/rice residue–lysine                      | N-CQDs            | 23.48%          | 360/440 nm                                   | 3.32–32.26 $\mu\text{M}$ | 0.7462 $\mu\text{M}$ | [46]      |
| CQDs/trisodium citrate–phosphoric acid        | P-CQDs            | 16.1%           | 310/440 nm                                   | 0.02–3 $\mu\text{M}$     | 9.5 nM               | [49]      |
| CQDs from cranberry                           | Pristine CQDs     | 10.85%          | 380/450 nm                                   | 30–600 $\mu\text{M}$     | 9.55 $\mu\text{M}$   | [62]      |
| CQDs from magnolia flower                     | N-CQDs            | 8.13%           | 350/435 nm                                   | 0.2–100 $\mu\text{M}$    | 0.073 $\mu\text{M}$  | [64]      |
| CQDs/carboxymethylcellulose–LPEI <sup>1</sup> | N-CQDs            | 44.0%           | 350/465.5 $\pm$ 3 nm                         | 1–400 $\mu\text{M}$      | 0.14 $\mu\text{M}$   | [86]      |
| CQDs/cellulose fiber–sulfuric acid            | S-CQDs            | 32.0%           | 360/435 nm                                   | 25–250 $\mu\text{M}$     | 0.96 $\mu\text{M}$   | [87]      |
| CQDs from <i>Fusobacterium nucleatum</i>      | N-CQDs            | 9.99%           | 360/450 nm                                   | 20–180 $\mu\text{M}$     | 0.82 $\mu\text{M}$   | [88]      |
| CQDs/glutamic acid–EDA <sup>2</sup>           | N-CQDs            | 12.45%          | 360/459 nm                                   | 8–80 $\mu\text{M}$       | 3.8 $\mu\text{M}$    | [89]      |
| CQDs/phenylalanine–citric acid                | N-CQDs            | ND <sup>3</sup> | 335/440 nm                                   | 5–500 $\mu\text{M}$      | 0.720 $\mu\text{M}$  | [90]      |
| CQDs/Trisodium citrate–urea–boric acid        | B,N-co-doped CQDs | 70.0%           | 340/450 nm                                   | 0–100 $\mu\text{M}$      | 80.0 $\pm$<br>0.5 nM | [91]      |
| CQDs/glutamic acid                            | N-CQDs            | 17.8%           | 370/440 nm                                   | 0–50 $\mu\text{M}$       | 4.67 $\mu\text{M}$   | [92]      |

|   |                   |                 |            |                   |                 |       |
|---|-------------------|-----------------|------------|-------------------|-----------------|-------|
| CQDs/EDA–microcrystalline cellulose                       | N-CQDs            | 51.0%           | 360/436 nm | 10–240 $\mu$ M    | 0.21 nM         | [93]  |
| CQDs/citric acid–L-cysteine                               | N,S-co-doped CQDs | 69.0%           | 345/415 nm | 1–500 $\mu$ M     | 0.014 $\mu$ M   | [94]  |
| CQDs/biomass tar–EDA                                      | N-CQDs            | 26.1%           | 340/420 nm | 0.06–1400 $\mu$ M | 60 nM           | [95]  |
| CQDs/watermelon juice–ethanol                             | N-CQDs            | 10.6%           | 355/439 nm | 0–300 $\mu$ M     | 0.16 $\mu$ M    | [96]  |
| CQDs/jujube fruit   | N-CQDs            | ND <sup>3</sup> | 370/440 nm | 0–200 $\mu$ M     | ND <sup>3</sup> | [97]  |
| CQDs/lignin in DES <sup>4</sup> (betaine and lactic acid) | N-CQDs            | 7.95%           | 300/400 nm | 0–500 $\mu$ M     | 0.44 $\mu$ M    | [98]  |
| CQDs/glucose–ammonia–phosphoric acid                      | N,P-co-doped CQDs | 30.0%           | 336/437 nm | 5–100 nM          | 1.8 nM          | [99]  |
| CQDs/tartaric acid–L-arginine                             | N-CQDs            | 8.3%            | 350/425 nm | 0–70 $\mu$ M      | 0.50 $\mu$ M    | [100] |

<sup>1</sup> LPEI—polyethyleneimine, <sup>2</sup> EDA—ethylenediamine, <sup>3</sup> ND—no data presented, <sup>4</sup> DES—deep eutectic solvent.

Furthermore, in the study by Shi et al. [99], the sensitive detection of Fe<sup>3+</sup> ions was achieved by using N,P-doped carbon quantum dots (N,P-co-doped CQDs). The synthesis of N,P-co-doped CQDs was performed by the hydrothermal method using glucose, ammonia, and phosphoric acid as precursors. The monodisperse nanoparticles of average size diameter of 3.0 nm exhibited a high quantum yield of QY = 30.0%. Furthermore, the XPS survey spectrum showed that C 1s, N 1s, P 2s, P 2p, and O 1s signals appeared at 285.0, 398.5, 188.8, 132.9, and 530.5 eV. The presence of N atoms was confirmed by the presence of two main peaks in the N 1s spectrum indicating the binding energy at 399.3 eV for the N-H bond and at 401.1 eV for C–N/N–N/N–P bond. The presence of P atoms was demonstrated by two main peaks located at 133.0 eV and 133.8 eV, corresponding to bonds between P–O and P–C/P–N. Regarding the optical characteristics of prepared N,P-co-doped CQDs, the fluorescence spectral studies indicated a red shift in the emission peak as the excitation wavelength increased from 316 to 406 nm, which could be attributed to the different sizes of nanoparticles and surface states [74,99]. The preliminary test results indicated potential sensing of Fe<sup>3+</sup> ions, while significant quenching of N,P-co-doped CQDs was observed in the presence of Cu<sup>2+</sup> ions. This potentially occurred due to the greater binding affinity and chelating kinetics between N/O functional groups of N,P-co-doped CQDs and Cu<sup>2+</sup>, as well as Fe<sup>3+</sup> ions. However, triethanolamine (TEA) could be used as a Cu<sup>2+</sup> chelating agent to reduce quenching effects in the presence of Cu<sup>2+</sup> ions. A good linear relationship with the Fe<sup>3+</sup> concentration was obtained within the concentration range of 5–100 nM ( $R^2 = 0.9958$ ) with an LOD = 1.8 nM. The assay with N,P-co-doped CQDs was also validated for the detection of Fe<sup>3+</sup> in human serum samples by the standard addition method and in the intracellular imaging of Fe<sup>3+</sup> ions. In the case of Fe<sup>3+</sup> analysis in human serum, the experimental results were in a good agreement with the spiked concentrations (RSD < 3.2%), while the low cytotoxicity of N,P-co-doped CQDs demonstrated potential semiquantitative imaging of Fe<sup>3+</sup> ions in living cells.

Nevertheless, an appropriate precursor or dopant selection in the CQDs fabrication plays a significant role in improving the selectivity and sensitivity toward Fe<sup>3+</sup> detection, as well as chemical stability in different pH environments.

## 5.2. Mercuric (Hg<sup>2+</sup>) Ions Detection

Mercury (Hg<sup>2+</sup>) ions are classified as nonessential and extremely toxic metal ions, representing a serious concern for the environment and human welfare. Even at lower concentration, Hg<sup>2+</sup> ions could represent high ecological and health risks due to their toxicity and bioaccumulation. A list of the novel CQDs-based sensors for the detection of Hg<sup>2+</sup> ions are summarized in Table 4. The N-CQDs-based sensor was developed by Zhu et al. [100] using tartaric acid and L-arginine as precursors. The nanoparticles were synthesized by solvothermal method in ethanol at temperature of 180 °C for 12 h, and fluorescence QY was calculated as QY = 8.3%. Under the excitation wavelength of  $\lambda_{EX} = 350$  nm, the maximum emission wavelength of N-CQDs at  $\lambda_{EM} = 425$  nm was observed. In addition, red-

shift was observed by increasing excitation wavelengths from 350 to 400 nm. A TEM measurement has confirmed monodisperse and well-uniformed nanoparticles with average diameter of 1.3 nm. In the reported work, the prepared N-CQDs were used for the detection of  $\text{Hg}^{2+}$  and  $\text{Fe}^{3+}$  ions (Figure 4). It was also found that the pH of the media has a significant effect on the sensing of mercury ions, as quenching intensity increases within the pH range from pH 3 to 7, and a significant decrease was observed from pH 7 to 11 [100]. This phenomenon could be explained by electrostatic repulsions between  $\text{Hg}^{2+}$  ions and protonated N-CQDs preventing the formation of the N-CQDs- $\text{Hg}^{2+}$  complex in the extreme acidic media, which causes quenching. However, under the extreme alkaline conditions, hydrolysis of the mercury ions occurs, causing the decrease in quenching efficiency. The significant influence of the pH media on the  $\text{Fe}^{3+}$  ion detection is not observed. Hence, pH = 7 was used as the optimal pH media for further investigation. The main problem was the ability of distinguishing the  $\text{Fe}^{3+}$  and  $\text{Hg}^{2+}$  ions in real sample analysis. It was found that the addition of thiourea can distinguish  $\text{Hg}^{2+}$  from  $\text{Fe}^{3+}$ , but this could lead to the fluorescence intensity enhancement. Only the addition of thiourea to N-CQDs solution did not affect the fluorescence intensity. The linear response for the  $\text{Hg}^{2+}$  ions was determined within the concentration range from 0 to 5  $\mu\text{M}$  with  $R^2 = 0.997$  and  $\text{LOD} = 0.017 \mu\text{M}$ . In the case of  $\text{Fe}^{3+}$  ions, the linear range was estimated from 0 to 70  $\mu\text{M}$  with  $R^2 = 0.993$  and  $\text{LOD} = 0.50 \mu\text{M}$ . The method was evaluated on the sensing of  $\text{Hg}^{2+}$  and  $\text{Fe}^{3+}$  ions in tap water by a standard addition method, and it was concluded that the method could achieve satisfactory results for determination of these two metals in a mixture solution.

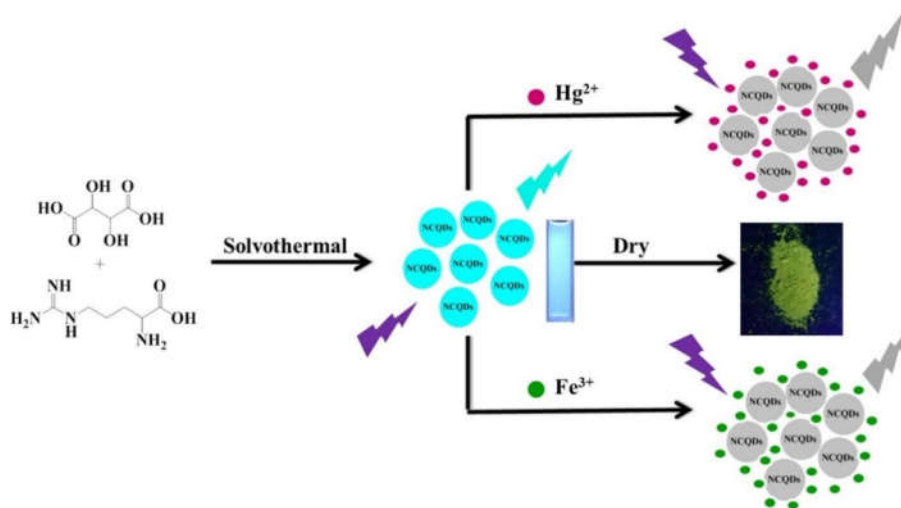


**Figure 4.** Schematic illustration of the preparation of N-CQDs using tartaric acid and L-arginine by a solvothermal method for dual sensing of  $\text{Hg}^{2+}$  and  $\text{Fe}^{3+}$  metal ions. Reprinted with permission from ref. [100]. Copyright 2020 Elsevier.

The development of a highly sensitive CQDs-based sensor toward  $\text{Hg}^{2+}$  ion detection was carried out by Huang et al. [101]. The biocompatible N-CQDs were prepared by hydrothermal treatment of a modified natural polymer, cellulose hydrogel. A cellulose was dissolved in NaOH/urea aqueous solution (7/12 wt %, 100 g, pre-cooled at  $-12 \text{ }^\circ\text{C}$ ), and epichlorohydrin (0.3 wt %) was added to the cellulose solution. After treatment at  $60 \text{ }^\circ\text{C}$  for 4 h, a crosslinked hydrogel was formed. The prepared hydrogel represented the precursor for the preparation of CQDs by hydrothermal synthesis at  $200 \text{ }^\circ\text{C}$  for 12 h. The product for further investigation was selected based on the performance after purification using dialysis bags with different molecular weight cut-off (MWCO) values (MWCO = 10 kDa and MWCO = 1.2 kDa) and the time period of CQDs being immersed in an aqueous NaOH-urea solution (7/12%, wt %; 48 h). After the CQDs/N-CQDs characterization, it was determined that the fluorescence QY of N-CQDs separated using a dialysis bag (MWCO

<1.2 kDa) and immersing cellulose hydrogel in an (7/12%, wt %) aqueous NaOH–urea solution for 48 h exhibited the highest QY = 18%. The N-CQD showed high selectivity toward Hg<sup>2+</sup> ions and two linear ranges within the concentration range from 0.2 to 10 μM ( $R^2 = 0.9948$ ) and from 10 to 100 μM ( $R^2 = 0.9911$ ). The limit of detection was estimated to be 0.2 μM.

**Table 4.** Summary of the literature reporting methods of Hg<sup>2+</sup> ions detection of the past five years (2016–2021).

| CQDs-Based Sensor   | Type of CQDs      | QY                                    | $\lambda_{EX}/\lambda_{EMmax}$                          | Linear Range   | LOD  | Reference |
|---|-------------------|---------------------------------------|---|--|--|-----------|
| CQDs from lemon juice/EDA   | N-CQDs            | 31.0%                                 | 360/452 nm  | 0.001–1 μM   | 5.3 nM   | [57]      |
| CQDs/tartaric acid–L-arginine                                       | N-CQDs            | 8.3%                                  | 350/425 nm  | 0–5 μM   | 0.017 μM                                       | [100]     |
| CQDs/cellulose hydrogel   | N-CQDs            | 18.3%                                 | 370/450 nm  | (i) 0.2 to 10 μM<br>(ii) 10 to 100 μM  | 0.2 μM   | [101]     |
| CQDs/citric acid–acrylamide–formamide                               | N-CQDs            | ND <sup>1</sup>                       | 560/644 nm  | 0–40 μM  | 0.19 μM  | [102]     |
| CQDs/hair   | N-CQDs            | 10.75%                                | 330/415 nm  | 0–75 μM  | 0.01 μM  | [103]     |
| CQDs/PAMAM <sup>2</sup> –APTES <sup>3</sup>                         | N-CQDs            | 52.6%                                 | 354/442 nm  | 0.2–15 nM  | 0.087 nM                                       | [104]     |
| CQDs/L-tryptophan   | N-CQDs            | 32.0%                                 | 350/440 nm  | 0–1.8 μM   | 10 nM<br>(in tap water)                        | [105]     |
| CQDs/citric acid–tartaric acid–ethanediamine                        | N-CQDs            | 42.2%                                 | 360/460 nm  | 0–18 μM  | 83.5 nM  | [106]     |
| Ag/CQDs composite   | Ag/CQDs           | ND <sup>1</sup>                       | ND <sup>1</sup>   | 0.5–50 μM  | 85 nM  | [107]     |
| CQDs/pigeon feathers (i), pigeon egg yolk (ii), and egg white (iii) | N,S-co-doped CQDs | (i) 24.8 %, (ii) 17.48%, (iii) 16.34% | (i) 330/415 nm,<br>(ii) 340/410 nm,<br>(iii) 340/420 nm | (i) 0 to 1.2 μM (pigeon feathers),<br>(ii) 0.05 to 1.2 μM (pigeon egg white),<br>(iii) 0 to 1.6 μM (pigeon egg yolk) | (i) 10.3 nM,<br>(ii) 34.6 nM,<br>(iii) 34.9 nM | [108]     |
| CQDs/sodium citrate–urea  | N-CQDs            | ND <sup>1</sup>                       | 390/450 nm  | 0.20–21 μM   | 3.3 nM   | [109]     |
| CQDs/ <i>Tamarindus indica</i> leaves                               | N-CQDs            | 46.6%                                 | 320/420 nm  | 0–0.1 μM   | 6 nM   | [110]     |
| CQDs/folic acid–glycerol–chloroauric acid                           | Au/N-CQDs         | 8.6%                                  | 355/450 nm  | 0–41.9 μM  | 0.118 μM                                       | [111]     |
| CQDs/glucose–aspartic acid–branched polyethyleneimine               | N-CQDs            | 45.0%                                 | 365/440 nm  | 20–800 nM  | 10 nM  | [112]     |
| CQDs/ <i>Prosopis juliflora</i> leaves                              | N-CQDs            | 5.0%                                  | (i) 325/396 nm<br>(ii) 350/437 nm                       | 5–500 ng/mL  | 1.26 ng mL <sup>-1</sup>                       | [113]     |
| CQDs/citric acid–glycine  | N-CQDs            | ND <sup>1</sup>                       | 350/432 nm  | 0.12–2 ppm   | 38 ppb   | [114]     |

<sup>1</sup> ND—no data presented, <sup>2</sup> PAMAM—polyamidoamine, <sup>3</sup> APTES—(3-Aminopropyl)triethoxysilane.

An interesting example of Hg<sup>2+</sup> sensing was presented in the study by Ye et al. [108] using N,S-co-doped CQDs as a fluorescent nanoprobe. The N,S-co-doped CQDs were synthesized via the pyrolysis carbonization method from pigeon feathers (PCQDs-f), pigeon egg yolk (PCQDs-y), pigeon egg white (PCQDs-w), and pigeon manure (PCQDs-m). The samples were placed in a muffle furnace and heated at 300 °C for 3 h. The obtained CQDs were purified by centrifugation and dialysis against distilled water for 4 days. Structural and morphological analysis confirmed a spherical particle shape with narrow size distribution, while XPS revealed that the PCQDs-w, PCQDs-y, and PCQDs-m comprised of carbon, oxygen, nitrogen, and sulfur elements. All obtained PCQDs exhibited high quantum yields compared to other works dealing with CQDs preparation from biomass. The QYs were determined as follows: QY = 24.87% for PCQDs-f, 17.48% for PCQDs-w, QY = 16.34% for PCQDs-y, and QY = 33.50% for PCQDs-m. When using PCQDs-m in selectivity tests, it was found that Ag<sup>+</sup>, Cu<sup>2+</sup>, and Hg<sup>2+</sup> can significantly quench the fluorescence of the PCQDs-m, while PCQDs-f was selected for further use in Hg<sup>2+</sup> sensing as the best-

performing fluorescent nanoprobe. While dual sensing of  $\text{Hg}^{2+}$  and  $\text{Fe}^{3+}$  was observed, it was found that the ions could be distinguished when using different buffer solutions. Hence, when using PCQDs-f in 4-(2-hydroxyethyl)-1-piperazineethanesulfonic acid (HEPES) solution,  $\text{Hg}^{2+}$  efficiently quenches the fluorescence of PCQDs-f, while almost no quenching was observed under the same conditions in the case of  $\text{Fe}^{3+}$  ion sensing. The possible mechanism toward  $\text{Hg}^{2+}$  sensing was attributed to the stronger affinity of  $\text{Hg}^{2+}$  toward carboxylic groups of the PCQDs surface compared to other metal ions. The developed method using PCQDs-f for the purpose of  $\text{Hg}^{2+}$  sensing showed good linearity within the 0–1.2  $\mu\text{M}$  concentration range with an obtained LOD = 10.3 nM. The method was also applied for monitoring  $\text{Hg}^{2+}$  in living cells, which showed great potential of using biomass-derived CQDs for biological studies. A fluorescent gold and nitrogen co-doped carbon quantum dots-based (Au/N-CQDs) nanoprobe for  $\text{Hg}^{2+}$  ion sensing was prepared by Meng et al. [111]. The Au/N-CQDs were prepared by a hydrothermal method using folic acid, glycerol, and chloroauric acid as precursors, which were treated at 180 °C for 12 h. The obtained nanoparticles were of average particle size of  $4.01 \pm 1$  nm, containing both crystalline and amorphous carbon. In addition, folic acid and glycerol introduced a number of functional groups, such as  $-\text{NH}_2$ ,  $-\text{COOH}$ , and  $-\text{OH}$ , which contributed to the enhancement of the optical properties. The examination of the optical properties demonstrated that as-prepared Au/N-GQDs exhibited the excitation-dependent fluorescence behavior with the maximum excitation ( $\lambda_{\text{EXmax}}$ ) and emission ( $\lambda_{\text{EMmax}}$ ) at 355 and 450 nm, while quantum yield was calculated to be  $\text{QY} = 8.6\%$ . Finally, Au/N-GQDs sensors showed high selectivity toward  $\text{Hg}^{2+}$  detection, and good linearity was obtained in the concentration range from 0 to 41.86  $\mu\text{M}$  ( $R^2 = 0.997$ ) and LOD = 0.118  $\mu\text{M}$ . The method was validated in the real water analysis, and good agreement between the expected and experimental results was obtained. The fluorescence lifetime analysis suggested that the quenching of Au/N-GQDs containing  $\text{Hg}^{2+}$  ions occurred through a dynamic quenching sensing mechanism.

### 5.3. Other Metals Ions Detection

The zinc ( $\text{Zn}^{2+}$ ) ions are considered an essential element in the human body, playing an important role in immunity and other biological functions, while it is well known that  $\text{Zn}^{2+}$  ions have an indispensable role in many enzymes [14]. The recent reports of the CQDs-based sensors for the detection of  $\text{Zn}^{2+}$  ions are summarized in Table 5. Recently,  $\text{Zn}^{2+}$ -passivated CQDs were prepared from zinc gluconate by the one-step pyrolysis reported by Yang et al. [115]. The prepared sensor was characterized as a reversible “off-on” fluorescent nanosensor for ethylenediaminetetraacetic acid (EDTA) and  $\text{Zn}^{2+}$  sensing. The CQDs were prepared by the calcination of glucose (G-CQDs) or zinc gluconate (Zn-CQDs) at 160 °C for 1 h at a heating rate of 5 °C/min under a  $\text{N}_2$  atmosphere. An interesting observation was made regarding the determination of QY. The fluorescence quantum yield of G-CQDs was calculated to be  $\text{QY} = 0.78\%$ , while for the Zn-CQDs, it was  $\text{QY} = 13.89\%$ , which is comparable to the modified CQDs, as shown in Table 2. The XPS, TEM, XRD, and FTIR analysis have shown that the  $\text{Zn}^{2+}$  ions had two important roles: (i) due to the formed zinc carboxylate groups, aggregation was prevented, and (ii)  $\text{Zn}^{2+}$  on Zn-CQDs acted as a passivation agent of surface defects, improving PL intensity, which will further be used for re-passivation. Hence, after it was shown that zinc ions were removed with the gradual addition of EDTA ions, a quenching effect was obvious. A good linearity was obtained within a 2.5–25  $\mu\text{M}$  concentration range with obtained  $R^2 = 0.9993$  and LOD = 0.32  $\mu\text{M}$ . However, by adding  $\text{Zn}^{2+}$  ions, a re-passivation of Zn-CQDs occurs. This phenomenon can be used for the sensing of  $\text{Zn}^{2+}$  ions. The linear range was obtained from 2 to 15  $\mu\text{M}$ , with  $R^2 = 0.9984$  and LOD = 0.51  $\mu\text{M}$ . It is suggested that after EDTA removes zinc ions, the lack of  $\text{Zn}^{2+}$  ions could lead to the PL quenching, leaving vacant positions for  $\text{Zn}^{2+}$  ions, while adding  $\text{Zn}^{2+}$  ions could lead to the re-passivation. This means that Zn-CQDs could be a reversible and efficient nanosensor for the selective detection of EDTA

and Zn<sup>2+</sup> ions. Similarly, S-,N-co-doped carbon quantum dots (SNCQDs) have been prepared by the solvothermal route using *p*-phenylenediamine and cysteamine hydrochloride as the precursors [116]. Interestingly, prepared monodispersed nanoparticles (less than 5 nm in size) emitted yellow/green luminescence and wavelength-independent behavior with a maximum excitation/emission wavelength at 420/550 nm. The red-shift was observed when excited by excitation wavelengths from 370 to 490 nm. It was suggested that strong luminescence originates from the emissive traps on the S- and N-co-doped surface. The prepared SNCQDs were used for the sensing of hypochlorous acid (HOCl) and Zn<sup>2+</sup> ions. For the sensing of HOCl, a linear range was obtained within the 0.18–4.22 μM concentration range, with  $R^2 = 0.9961$  and LOD = 0.021 μM. It is shown that HOCl causes a quenching effect and slight blue-shift of the emission maximum. Again, by adding Zn<sup>2+</sup> ions, recovery of the sensing system occurs and can be used for the detection of Zn<sup>2+</sup> ions. This phenomenon can be explained by the higher affinity of Zn<sup>2+</sup> ions for the HOCl rather than for the oxygen/sulfur/nitrogen functional groups on the SNCQDs surface. The linear range for the sensing of Zn<sup>2+</sup> ions was obtained from 8.41 to 84.12 μM, with  $R^2 = 0.9925$  and LOD = 0.30 μM.

**Table 5.** Summary of the literature reporting methods of miscellaneous metal ions detection of the past five years (2016–2021).

| CQDs-Based Sensor                                       | Type of CQDs            | QY                               | $\lambda_{EX}/\lambda_{EMmax}$ | Target Metal Ion | Linear Range                | LOD                      | Reference |
|---|-------------------------|----------------------------------|--------------------------------|------------------|-----------------------------|--------------------------|-----------|
| CQDs/potato starch                                      | Pristine CQDs           | 10.0%                            | 365/515 nm                     | Zn <sup>2+</sup> | 0–20 μM                     | 1 nM                     | [55]      |
| CQDs/onion extract                                      | N-CQDs                  | 10.85%                           | 380/450 nm                     | Zn <sup>2+</sup> | -                           | 6.4 μM                   | [63]      |
| CQDs/zinc gluconate                                     | Zn-CQDs                 | 13.89%                           | 365/460 nm                     | Zn <sup>2+</sup> | 2–15 μM                     | 0.51 μM                  | [115]     |
| CQDs/ <i>p</i> -phenylenediamine and cysteamine         | N,S-co-doped CQDs       | ND <sup>1</sup>                  | 420/550 nm                     | Zn <sup>2+</sup> | 0.18–4.22 μM                | 0.021 μM                 | [116]     |
| CQDs/broccoli   | N-CQDs                  | ND <sup>1</sup>                  | 355/450 nm                     | Ag <sup>+</sup>  | 0–600 μM                    | 0.5 μM                   | [117]     |
| CQDs/MWCNTs <sup>2</sup> -amine and thiol modifications | CQDs hydrogels          | ND <sup>1</sup>                  | 350/430 nm                     | Ag <sup>+</sup>  | 0.8–20 μg mL <sup>-1</sup>  | 0.55 μg mL <sup>-1</sup> | [118]     |
| CQDs/osmanthus fragrans                                 | N-CQDs                  | 21.9%                            | 350/435 nm                     | Al <sup>3+</sup> | 0.1–100 μM                  | 26 nM                    | [119]     |
| CQDs/prickly pear cactus juice                          | GSH <sup>3</sup> -CQDs  | 12.7%                            | 355/446 nm                     | As <sup>3+</sup> | 2–12 nM                     | 2.3 nM                   | [120]     |
| CQDs/jackfruit seeds- <i>o</i> -phosphoric acid         | N-CQDs                  | 17.91%                           | 360/437 nm                     | Au <sup>3+</sup> | 0–100 μM                    | 239 nM                   | [121]     |
| CQDs/citric acid-EDA <sup>4</sup> -EGTA <sup>5</sup>    | N-CQDs                  | ND <sup>1</sup>                  | 360/460 nm                     | Ca <sup>2+</sup> | 15–300 μM                   | 0.38 μM                  | [122]     |
| CQDs/EDTA <sup>6</sup>                                  | N-CQDs                  | 22.0%                            | 353/450 nm                     | Ca <sup>2+</sup> | 1–10 nM                     | 77 pM                    | [123]     |
| CQDs/alanine-histidine                                  | CQDs-AuNCs <sup>7</sup> | 20.02%                           | 340/438 nm                     | Cd <sup>2+</sup> | 0.4–15 μM                   | 32.5 nM                  | [124]     |
| CQDs/glycine-PEI <sup>8</sup>                           | N-CQDs                  | 57.0%                            | 365/464 nm                     | Co <sup>2+</sup> | 0.5–3 μM                    | 0.12 μM                  | [125]     |
| CQDs/edible seeds                                       | Pristine CQDs           | 41.8% (the best performing CQDs) | 347/421 nm                     | Cr <sup>3+</sup> | 1–14 μM                     | 1.3 μM                   | [126]     |
| CQDs/citric acid-L-reduced GSH <sup>3</sup>             | N-CQDs                  | 69.0%                            | 350/418 nm                     | Cr <sup>6+</sup> | 0.10–12 μg mL <sup>-1</sup> | 0.03 μg mL <sup>-1</sup> | [127]     |
| CQDs/tuberose ( <i>Polygonatum tuberosum</i> L.)        | N-CQDs                  | 3.0%                             | 330/430 nm                     | Cu <sup>2+</sup> | 0–70 μM                     | 200 nM                   | [128]     |
| CQDs/waste polyolefin                                   | Pristine CQDs           | 4.84%                            | 490/540 nm                     | Cu <sup>2+</sup> | 1–8 μM                      | 6.33 nM                  | [129]     |
| CQDs/citric acid-L-cysteine                             | N,S-co-doped CQDs       | 82.0%                            | 375/430 nm                     | Cu <sup>2+</sup> | 0.01–0.5 μg L <sup>-1</sup> | 2.1 μg L <sup>-1</sup>   | [130]     |
| CQDs/Finger millet ragi ( <i>Eleusine coracana</i> )    | N-CQDs                  | ND <sup>1</sup>                  | 340/425 nm                     | Cu <sup>2+</sup> | 0–100 μM                    | 10 nM                    | [131]     |
| CQDs/prawn shell  | N-CQDs                  | 9.0%                             | 330/405 nm                     | Cu <sup>2+</sup> | 0.1–5 μM                    | 5 nM                     | [132]     |

|   |                |                 |            |                  |             |         |       |
|---|----------------|-----------------|------------|------------------|-------------|---------|-------|
| CQDs/durian shell waste-urea-aluminum nitrate | N/Al-CQDs      | 28.7%           | 345/415 nm | Mn <sup>7+</sup> | 0–100 µM    | 46.8 nM | [133] |
| CQDs/citric acid-urea-imidazole               | CQDs-imidazole | ND <sup>1</sup> | 360/435 nm | Ni <sup>2+</sup> | 6–100 mM    | 0.93 mM | [134] |
| CQDs/sodium citrate-polyacrylamide            | N-CQDs         | 18.0%           | 343/434 nm | Pb <sup>2+</sup> | 0.0167–1 µM | 4.6 nM  | [135] |
| CQDs/lemon juice                              | Pristine CQDs  | 21.0%           | 420/540 nm | V <sup>5+</sup>  | 0–8 ppm     | 3.2 ppm | [136] |

<sup>1</sup> ND—no data presented, <sup>2</sup> MWCNTs—multi-walled carbon nanotubes, <sup>3</sup> GSH—glutathione, <sup>4</sup> EDA—ethylenediamine, <sup>5</sup> EGTA—ethylenebis-(oxyethylenitrilo)tetraacetic acid, <sup>6</sup> EDTA—ethylenediaminetetraacetic acid, <sup>7</sup> AuNCs—gold nanoclusters, <sup>8</sup> PEI—polyethylenimine.

Moreover, the determination of aluminum (Al<sup>3+</sup>) in biological and environmental systems is of a great importance as it could significantly affect the quality of living and human health. Hence, in the study of Yu et al. [119], the preparation of N-CQDs for the Al<sup>3+</sup> and quercetin (QT) detection was reported. The N-CQDs were fabricated by a facile hydrothermal procedure using a natural carbon source, *osmanthus fragrans*. The hydrothermal synthesis was carried out in a Teflon-lined autoclave at 180 °C for 10 h. The obtained N-CQDs exhibited a high quantum yield of QY = 21.9% (quinine sulfate was used as a reference standard), strong fluorescence, and water solubility. An interesting observation was made regarding the affinity of N-CQDs toward binding quercetin and/or Al<sup>3+</sup> ions. Due to the presence of a  $\pi$ -bonding conjugated system and strong coordination of oxygen (O) atoms, quercetin could interact with Al<sup>3+</sup> ions to form a QT–Al<sup>3+</sup> complex. This means that the N-CQDs/QT system could be used for the detection of Al<sup>3+</sup> ions. As QT was introduced to N-CQDs solution, fluorescence quenching was observed. The sensing mechanism related to quercetin detection was proposed, and it was concluded that an inner filter effect (IFE) and static quenching effect are responsible for the fluorescence behavior of the N-CQDs–QT system, as zeta-potential measurements indicated that no complexation could occur (the zeta potential of N-CQDs aqueous solution was determined to be –6.18 mV, and that of QT was –10.8 mV). The addition of Al<sup>3+</sup> ions caused the fluorescence recovery of the N-CQDs/QT system, while no changes in the fluorescence emission intensity were observed when Al<sup>3+</sup> was added to the N-CQDs solution. Using the N-CQDs/QT system, a linear concentration range of Al<sup>3+</sup> was determined from 0.1 to 100 µM, with an estimated LOD = 26 nM. The sensing of Al<sup>3+</sup> was evaluated in real system analysis, human serum, and living cells. The obtained RSD results less than 3.4% indicated good accuracy and method precision with potential application in dual sensing of quercetin and Al<sup>3+</sup>, especially in the biomedical field. The detection of arsenic (As<sup>3+</sup>) ions is of crucial importance for environmental analysis and water quality assessment. Long-term exposure to arsenic in drinking water can cause adverse health effects and threaten the public health and environment. A synthetic procedure of glutathione-passivated CQDs (GSH-CQDs) used for As<sup>3+</sup> detection is shown in Figure 5, and it was reported by Radhakrishnan and Panneerselvam [120].



**Figure 5.** Illustration of synthetic route for obtaining GSH-CQDs and working principle toward the sensitive detection of As<sup>3+</sup> metal ions [120].

The GSH-CQDs were prepared by a hydrothermal method using prickly pear cactus juice and aqueous ethanolic solution (1:1, *v/v*), while GSH was added to the prepared mixture and refluxed for 1 h. The hydrothermal synthesis was carried out at 180 °C for 12 h. The obtained GSH-CQDs exhibited good quantum yield of QY = 12.7%, and zeta-potential measurements resulted in a negative-charged surface (−26.28 mV), indicating that the functionalization of the carboxylic groups on the surface of GSH-CQDs occurred. The influence of pH on the PL intensity was investigated, and it was found that the neutral medium contributed to the maximum emission PL intensity, indicating that the sensitive detection of As<sup>3+</sup> could be achieved by GSH-CQDs in drinking water samples. A linear range for As<sup>3+</sup> detection was determined within the concentration range from 2 to 12 nM, with an estimated LOD = 2.3 nM. It is proposed that fluorescence quenching is attributed to the formation of As–O on the surface of GSH-CQDs, showing the good ability of prepared CQDs for chelation with ions. The developed method was evaluated in the real water analysis. The obtained recovery values of As<sup>3+</sup> showed good agreement in spiked samples in environmental water analysis. An ultra-sensitive detection of Ca<sup>2+</sup> in human serum using multi-carboxylic acid-functionalized CQDs was achieved by Ankireddy et al. [123]. The multi-carboxylic acid-functionalized CQDs were prepared by hydrothermal treatment using ethylenediaminetetraacetic acid (EDTA) at 170 °C for 3 h. The obtained monodisperse particle of average diameter size of 3–5 nm mainly consisted of carbon, oxygen, and nitrogen elements, which was confirmed by XPS analysis. A strong blue fluorescence was emitted with maximum excitation and emission wavelengths centered at  $\lambda_{EXmax} = 353$  nm and  $\lambda_{EMmax} = 450$  nm. A great stability in high ionic strength environments adjusted with NaCl solution indicated that prepared N-CQDs are stable under different physiological conditions and could be suitable for sensing and bio-imaging applications. As a result of the multiple carboxylate groups on the N-CQDs surface, pH is an important factor for the quenching efficiency of N-CQDs evaluation. At extreme acidic conditions, the carboxylate groups present on the N-CQDs surface are protonated, and the formation of a carboxylate–Ca<sup>2+</sup> complex is interrupted. Although, carboxylate groups are deprotonated, a carboxylate–Ca<sup>2+</sup> complex could be formed, and PL intensity quenching could occur in extreme alkaline conditions, weakly acidic media (pH 4–7.2) showed similar quenching efficiency, and it was suitable for Ca<sup>2+</sup> sensing in human serum. A higher linear relationship was demonstrated with Ca<sup>2+</sup> in human serum compared to Ca<sup>2+</sup> in deionized water, which indicated higher sensitivity in detecting Ca<sup>2+</sup> in human serum. The linearity for the detection of Ca<sup>2+</sup> ions in human serum was obtained in a concentration range from 1 to 10 nm with LOD = 77 pM. A PL quenching mechanism was proposed relating the surface charge states of N-CQDs particles and the possibility of complex formation in the presence

of  $\text{Ca}^{2+}$  ions. Zeta-potential measurements of the as-prepared N-CQDs indicated that the surface was functionalized with negative-charged functional groups such as carboxylic acids ( $-10.09$  mV). The addition of  $\text{Ca}^{2+}$  ions caused the shift of zeta potential toward less negative values of  $-2.42$  mV due to the formation of a  $[\text{Ca-EDTA}]^{2-}$  octahedral complex on the N-CQDs surface. It was suggested that PL quenching occurs via a non-radiative electron or energy transfer process. This hypothesis was also confirmed by the time-resolved PL lifetime decay analysis and the band gap ( $E_g$ ) determination.

## 6. Photoluminescent Sensing of Molecules

Although the synthesis and application of different CQDs is mostly related to the ion sensing in the literature, there is also an enormous potential for the sensing of different molecules or biomolecules. The list of recent published works based on the CQDs sensors for the detection of different (bio)molecules is given in Table 6. A biosensor for the selective detection of Gram-negative bacteria *Escherichia coli* (*E. coli*) was developed by Chandra et al. [137]. A CQDs-based sensor was prepared using di-ammonium hydrogen citrate and colistin sulfate in order to obtain colistin conjugated CQDs. Colistin is a medication classified as a bactericidal drug that interacts with lipopolysaccharide (LPS) molecules in the outer membrane of the *E. coli* bacteria cell. The developed CQDs@colistin conjugate showed good stability in the pH range from pH 5 to 9. The calculated QY was estimated to be 7.56% for the CQDs@colistin conjugate and for pristine CQDs (without colistin), QY was estimated as 11.21%. It is interesting that CQDs@colistin exhibited lower fluorescence QY, which was possibly due to the presence of colistin on the CQDs surface, interfering with the radiative recombination of the excitons and giving rise to lower fluorescence. Hence, the prepared CQDs@colistin was investigated for the sensing of  $\text{Fe}^{3+}$  ions and *E. coli*. The linear relationship was observed from  $3.81 \times 10^2$  to  $2.44 \times 10^4$  cfu/mL, with  $R^2 = 0.995$  and  $\text{LOD} = 460$  cfu/mL. The prepared biosensor showed a good performance of the antibiotic drug conjugated N-CQDs toward detecting and labeling *E. coli* bacteria cells. The application of CQDs in the antibiotics detection was reported by Qi et al. [46], more precisely in the detection of tetracyclines, which are broad-spectrum antibiotics used in veterinary and human medicine with potential risks of accumulation in food products. The biomass-derived N-CQDs were synthesized by hydrothermal treatment using rice residue and amino acid lysine at  $200$  °C during 12 h. The fluorescence QY of the N-CQDs was calculated to be  $\text{QY} = 23.48\%$ . Nanoparticles with an average size of 2.70 nm demonstrated good photostability, biocompatibility, high fluorescence, and excellent solubility in water. At an excitation wavelength of  $\lambda_{\text{EX}} = 360$  nm, an emission fluorescence maximum was observed at  $\lambda_{\text{EM}} = 440$  nm. The linear relationship was observed from 3.32 to 32.26  $\mu\text{M}$  in tetracycline detection, obtaining  $R^2 = 0.983$  and  $\text{LOD} = 0.2367$   $\mu\text{M}$ . In addition, the prepared nanoparticles were investigated for the  $\text{Fe}^{3+}$  ion detection in polluted water, as well as for cytotoxicity, and cellular imaging showing good performance.

An interesting example for presenting versatile application of the CQDs as a biosensor is the detection of influenza A (H1N1) virus reported by Achadu et al. [48]. The sensing was based on the conjugation of specific antihuman influenza A monoclonal antibody to the sulfur-doped graphitic carbon nitride CQDs (S-gCNQDs) and  $\text{Ag}_2\text{S}$  nanocrystals. The S-gCNQDs were prepared by solvothermal treatment of 4-amino-3-hydrazino-5-mercapto-1,2,4-triazole and citric acid dissolved in DMF, and the mixture was heated at  $200$  °C for 8 h. The final product was purified by filtration and dialysis ( $\text{MWCO} = 2$  kDa) and then freeze dried for further use. The structural analysis confirmed quasi-spherical morphology of S-gCNQDs within the size range from 3 to 5 nm. When excited to the wavelength  $\lambda_{\text{EX}} = 400$  nm, a strong green luminescence was emitted at  $\lambda_{\text{EM}} = 512$  nm, and QY was estimated to  $\text{QY} = 33\%$  in aqueous solution. Selective and sensitive sensing of H1N1 virus was performed using a designed nanocomplex comprised of antibody-conjugated S-gCNQDs and antibody- $\text{Ag}_2\text{S}$  nanocrystals. The linear range was observed within the concentration range from 10 fg/mL to 1 ng/mL, with  $R^2 = 0.9872$  and  $\text{LOD} = 5.5$  fg/mL measured in deionized water. The sensor was also tested on the detection of H1N1 virus

measured in human serum. The LOD was estimated to be 8.5 fg/mL in human serum. In order to detect clinically isolated virus of influenza A (H3N2), the S-gCNQDs were modified with H3N2 monoclonal antibody in the presence of antibody-Ag<sub>2</sub>S nanocrystals to form a nanosandwich complex. It was concluded that the biosensor demonstrated high sensitivity and selectivity toward the target virus and presented potential application in rapid sensing of very infectious diseases. Interestingly, there are few reports of the potential use of carbon dots in antiviral therapy and also for biosensing purposes, including biosensing of HIV DNA sequences [138,139]. A FRET-based DNA biosensor using single-stranded DNA (ss-DNA) functionalized CQDs as the energy donor and gold nanoparticles (AuNPs), AuNPs/graphene oxide (GO), as efficient quenchers demonstrated the efficiency down to the femtomolar level for the detection of HIV DNA (Figure 6). The detection limit for the HIV DNA method was estimated to be LOD = 15 fM. The method was evaluated for the analysis of real samples, in this case for the detection of HIV DNA in human serum, and it was concluded that immunoassay could be used for the efficient sensing of HIV in human serum. It is also suggested that this type of immunoassay could be also investigated for the detection of viral RNAs. As it can be noticed, there are some examples of the CQDs application in viral biosensing that could be of a great importance for the theranostic purpose. Most recently, the ongoing global pandemic of SARS-CoV-2 (coronavirus disease, COVID-19) has become the greatest challenge to modern science. It is well known that early, rapid, low-cost, and accurate diagnosis of SARS-CoV-2 is of great importance in order to prevent further spreading of the virus. Although there have not yet been any studies reported of using pristine or modified CQDs as a viral therapy to combat or for the detection of COVID-19, the above-reported examples are undoubtedly showing that carbon dots have a great potential for theranostic application against SARS-CoV-2 [138].

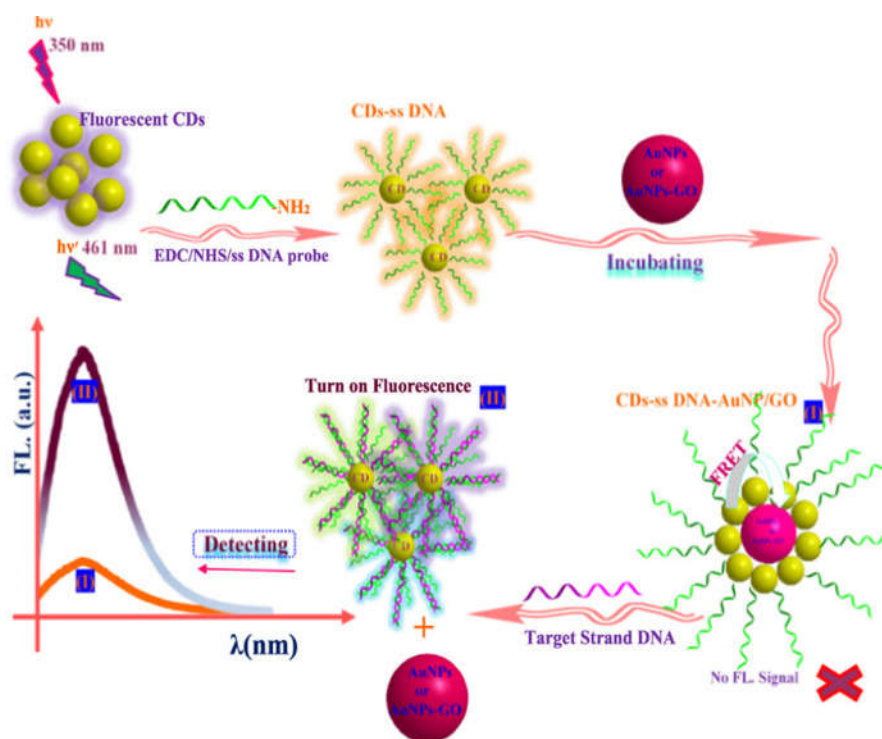


**Figure 6.** Schematic illustration of the fabrication of CQDs-ss DNA-AuNPs/GO for homogeneous HIV-1 gene detection at the femtomolar level. Reprinted with permission from ref. [139]. Copyright 2017 Elsevier.

**Table 6.** CQDs prepared from different carbon sources and their application in molecules sensing.

| Raw Material   | Synthesis/Modification   | QY              | $\lambda_{EX}/\lambda_{EMmax}$ | Analyte   | Linear Range  | LOD                          | Reference |
|--|--|-----------------|--------------------------------|---|---|------------------------------|-----------|
| Rice residue   | Hydrothermal/lysine  | 23.48%          | 360/440 nm                     | Tetracycline–antibiotic   | 3.32–32.26 $\mu\text{M}$  | 0.7462 $\mu\text{M}$         | [46]      |
| Arginine   | Hydrothermal   | 48.0%           | 360/430 nm                     | 4-chloroethcathinone–psychoactive substance                               | 2000–12500 $\text{ng mL}^{-1}$  | 1300 $\text{ng mL}^{-1}$     | [47]      |
| Fresh tomato   | Microwave-assisted synthesis/urea  | 8.5%            | 300/356 nm                     | Vanillin  | 3–55 $\mu\text{M}$  | 24.9 $\text{mg kg}^{-1}$     | [54]      |
| Mixture of lemon and onion juice                       | Microwave-assisted Carbonization/ $\text{NH}_4\text{OH}$                             | 23.6%           | 380/440 nm                     | Riboflavin  | 0.10–3.0 $\text{mg/mL}$   | 1.0 $\text{ng/mL}$           | [61]      |
| Citric acid monohydrate and tartaric acid              | One-step solvothermal  | 42.2%           | 360/460 nm                     | L-cysteine  | 0–40 $\mu\text{M}$  | 45.8 nM                      | [106]     |
| <i>Prosopis juliflora</i> leaves                       | Carbonization  | 5.0%            | 350/437 nm                     | Chemet (anti-poisoning drug for heavy metal ions)                         | 2.5–22.5 $\text{ng mL}^{-1}$  | 1.4 $\text{ng mL}^{-1}$      | [113]     |
| Osmanthus fragrans                                     | Hydrothermal   | 21.9%           | 350/435 nm                     | Quercetin (QT)  | 0.003–80 $\mu\text{M}$  | 1 nM                         | [119]     |
| Histidine in NaOH                                      | Hydrothermal   | ND <sup>1</sup> | 350/460 nm                     | HIV DNA   | 50.0 fM–1.0 nM  | 15 fM                        | [139]     |
| Citric acid  | Hydrothermal   | ND <sup>1</sup> | 320/430 nm                     | Kanamycin–antibiotic  | 0.04–0.24 mM  | 18 nM                        | [140]     |
|  | Hydrothermal/thiourea  | 24.0%           | 550/610 nm                     | Parathion–insecticide   | 0.1–10 mU $\text{mL}^{-1}$  | 0.0625 $\text{pg mL}^{-1}$   | [141]     |
|  | Hydrothermal/cysteine  | 57.2%           | 355/450 nm                     | Methotrexate–chemotherapy agent   | 0.4–41.3 $\mu\text{g/mL}$   | 12 $\text{ng/mL}$            | [142]     |
|  | Microwave-assisted synthesis/EDA–AuNPs <sup>2</sup>                                  | ND <sup>1</sup> | 360/455 nm                     | Paraoxon–insecticide  | (i) 0.01–1 $\mu\text{g L}^{-1}$ and (ii) 1.0–0.001 $\text{ng L}^{-1}$ | 1.0 $\text{ng L}^{-1}$       | [143]     |
| Citric acid–urea–DMF                                   | Solvothermal   | 5.5%            | 365/450 and 500 nm             | $\text{H}_2\text{O}_2$  | 0.05–0.5 M  | 14 mM                        | [144]     |
| Sucrose– $\text{H}_2\text{SO}_4$ –PEG 200 <sup>3</sup> | Reduction/CQDs–AuNPs <sup>1</sup>  | ND <sup>1</sup> | 420/527 nm                     | Malathion in cabbage  | $1 \times 10^{-9}$ – $1 \times 10^{-2}$ M                             | $0.13 \times 10^{-9}$ M      | [145]     |
| Ethylenediamine (EDA)                                  | Microwave-assisted synthesis/ $\beta$ -cyclodextrin functionalized N,Zn-co-doped CQD | 14.26%          | 350/480 nm                     | Ofloxacin–antibiotic  | 0.027–1.3537 $\mu\text{g mL}^{-1}$                                    | 0.0181 $\mu\text{g mL}^{-1}$ | [146]     |
| $\kappa$ -Carrageenan and urea                         | Hydrothermal   | 69.27%          | 360/432 nm                     | Acetone in human fluids   | 0–0.05 M (in blood) and 0–0.01 M (in urine)                           | 0.72 $\mu\text{M}$           | [147]     |
| <i>p</i> -aminobenzoic acid and ethanol                | Solvothermal   | ND <sup>1</sup> | 350/460 nm                     | Hematin in human red cells  | 0.5–10 $\mu\text{M}$  | 0.25 $\mu\text{M}$           | [148]     |
| Gelatin  | Hydrothermal   | 26.9%           | 330/436 nm                     | Atrazine, chlorpyrifos, imidacloprid, lindane and tetradifon–insecticides | Best performance for imidacloprid 0–17 mM                             | 0.013 mM                     | [149]     |
| Beet   | Hydrothermal   | ND <sup>1</sup> | ND <sup>1</sup>                | Amoxicillin–antibiotic  | 0–400 $\mu\text{M}$   | 0.475 $\mu\text{M}$          | [150]     |
| <i>o</i> -aminophenol                                  | Hydrothermal   | 40.0%           | 300/410 nm                     | Heparin–anticoagulant   | 10–100 nM   | 8.2 nM                       | [151]     |

|   |  |                 |                                 |  |   |  |       |
|---|--|-----------------|---------------------------------|--|---|--|-------|
| Melamine  | Hydrothermal/solvothermal treatment/molybdenum trioxide (MP-MoO <sub>3</sub> CQDs) | 44.0%           | 500/652 nm                      | Influenza A virus (H1N1)                     | 45–25000 PFU/mL   | 45 PFU/mL                                | [152] |
| 4-amino-3-hydrazino-5-mercapto-1,2,4-triazole           | Solvothermal synthesis/N-,S-doped CQDs   | 33.0%           | 400/512 nm                      |  | 10 fg/mL to 1.0 ng/mL   | 5.5 fg/mL                                | [48]  |
| <i>n</i> -(2-aminoethyl)-3-aminopropyl-trimethoxysilane | Co-hydrolysis/silanized CQDs with TEOS <sup>4</sup>                                | 56.3%           | 360/459 nm                      | SFTS <sup>5</sup> virus                      | Visual detection  | 10 pg/mL                                 | [153] |
| 4-hydroxy phenylboronic acid                            | Hydrothermal/B-doped CQDs  | 30.0%           | 295/398 nm                      | Dopamine                                     | (i) 0.28–1.5 mM and (ii) 1.32–2.5 mM                                | 6 μM                                     | [154] |
| L-cysteine and ammonia                                  | Hydrothermal/N,S-doped CQDs  | 17.2%           | 410/505 nm                      | Glutathione                                  | (i) 0–50 μM, and (ii) 50–100 μM                                     | 6.7 μM                                   | [155] |
| Lignin  | Hydrothermal   | 44.0%           | 350/465.5 nm                    | Ascorbic Acid (AA) and Fe <sup>3+</sup>      | For AA (i) 0–350 μM, and for Fe <sup>3+</sup> (ii) 50–650 μM        | (i) LOD = 5.34 μM, and (ii) LOD = 196 nM | [156] |
| Glutamic acid and citric acid                           | One-step pyrolysis   | 16.2%           | 360/448 nm                      | Ascorbic Acid (AA) and Cr <sup>6+</sup>      | For AA (i) 1.0–750 μM, and for Cr <sup>6+</sup> (ii) 0.01 to 250 μM | (i) LOD = 0.3 μM, and (ii) LOD = 5 nM    | [157] |
| (i) Citric acid–NaOH; (ii) malic acid–NaOH              | Chemical oxidation   | ND <sup>1</sup> | (i) 370/465 nm, (ii) 370/430 nm | DNA  | (i) 0.4–400 nM, and (ii) 0.04–400 nM                                | (i) 45.6 nM, and (ii) 17.4 nM            | [158] |
| Tris(hydroxymethyl)aminomethane and citric acid         | Pyrolysis/composite of CQDs/Fe <sub>3</sub> O <sub>4</sub> @APBA <sup>6</sup>      | 58.7%           | 332/407 nm                      | Glucose                                      | 0.2–20 mM   | 0.15 μM                                  | [159] |
|   | Hydrothermal   | ND <sup>1</sup> | 350/420 nm                      | Curcumin                                     | 5–30 μM   | 21.79 nM                                 | [160] |
| di-Ammonium hydrogen citrate                            | Pyrolysis/CQDs@colistin  | 7.56 %          | 360/450 nm                      | <i>Escherichia coli</i> ( <i>E. coli</i> )   | 3.81 × 10 <sup>2</sup> –2.44 × 10 <sup>4</sup> CFU mL <sup>-1</sup> | 460 CFU mL <sup>-1</sup>                 | [137] |
| Ammonium citrate-mannose                                | Solid-state synthesis  | 9.0 %           | 365/460 nm                      |  | 0–10 <sup>8</sup> CFU mL <sup>-1</sup>                              | 100 CFU mL <sup>-1</sup>                 | [161] |
| Pancreatin  | Hydrothermal/N-CQDs/aptamer/AuNPs <sup>2</sup>                                     | 26.8%           | 370/445 nm                      | Aflatoxin B <sub>1</sub> (AFB <sub>1</sub> ) | 0.005–2 ng mL <sup>-1</sup>   | 5 pg mL <sup>-1</sup>                    | [162] |

<sup>1</sup> ND—no data presented, <sup>2</sup> AuNPs—gold nanoparticles, <sup>3</sup> PEG 200—polyethylene glycol 200, <sup>4</sup> TEOS—tetraethyl orthosilicate, <sup>5</sup> SFTS—severe fever with thrombocytopenia syndrome, <sup>6</sup> APBA—3-amino phenylboronic acid.

Moreover, CQDs have also found many applications in food safety regarding the detection of different nutrients, toxins, and restricted substances or foodborne pathogenic bacteria. An interesting example of CQDs application in sensitive aflatoxin B<sub>1</sub> (AFB<sub>1</sub>) detection was reported by Wang et al. [162]. In this study, synthesized N-CQDs from pancreatin were assembled on aptamer/gold nanoparticles (AuNPs) by electrostatic interactions. The N-CQDs were prepared by the hydrothermal treatment of pancreatin at 180 °C for 10 h. The AuNPs were fabricated by the reduction of HAuCl<sub>4</sub> with trisodium citrate solution, when thiol-labeled DNA was attached onto the surface of AuNPs via the formation of Au-S or Au-N bonds. Finally, N-CQDs/aptamer/AuNPs nanocomposite was assembled, and fluorescence quenching was observed. It is suggested that with the addition of AFB<sub>1</sub>, specific binding of AFB<sub>1</sub> to the nucleic acid aptamer may weaken the binding between aptamer and N-CQDs, recovering the fluorescence emission. The linear range for AFB<sub>1</sub> detection using fluorescence measurements was determined in the 0.005–2.0 ng mL<sup>-1</sup> concentration range, with LOD = 5 pg mL<sup>-1</sup>. The method was assessed in real sample analysis of peanut and corn with average recoveries in the range of 92.00–105.00% and

RSD lower than 3%. These results are clearly indicating the potential application as an aptasensor for the sensing of target assay, whose selectivity depends on the aptamer used.

## 7. Electrochemical Sensors

Electrochemical methods are often used for CQDs synthesis due to their purity, low cost, high yield, and well-controlled synthesis conditions. The obtained CQDs can be functionalized by covalent and non-covalent modification of amino, carboxyl, and hydroxyl groups in CQDs to improve their properties. In Table 7, electrochemical synthesis conditions of different CQDs and their application in electrochemical sensing, cell imaging, photocatalysis, and supercapacitor electrode material are given. The CQDs have been used for electrode modification (mostly glassy carbon and screen-printed electrode) by the drop-casting method, in which CQDs dispersion was placed on the electrode surface, followed by drying. If the surface was dried at higher temperatures (with hair dryer or in the oven), the physicochemical adsorption of functional groups of CQDs on the electrode surface occurred. The resulting modified electrode has a large active area, which can be used for metal ions (e.g.,  $\text{Fe}^{3+}$ ) and organic molecules (e.g., dopamine, adrenaline, ascorbic acid etc.) detection, since the signal output was enhanced and the lower LOD values were obtained. In order to avoid the interferences, an additional layer (e.g., nafion layer) can be coated on the modified electrode surface [163].

**Table 7.** Electrochemical preparations of CQDs and their potential applications.

| Precursor                                     | Electrochemical Synthesis—Conditions  | QY<br>( $\lambda_{\text{EX}}/\lambda_{\text{EMmax}}$ ) | Modification Method<br>(CQDs/Electrode)   | Applications   | References |
|---|---|--|---|--|------------|
| Graphite rod                                  | Electrochemical synthesis; two graphite rods as working and counter electrode in electrolyte of ionic liquid (IL)   | 10.0%<br>(360/440 nm)                                  | -   | Bacteria cell imaging  | [164]      |
|   | Electrochemical synthesis; two graphite rods were used as anode and cathode in 0.1 M NaOH/EtOH electrolyte, constant current 50 mA was applied for 3 h  | ND <sup>1</sup><br>(ND <sup>1</sup> )                  | Glassy carbon electrode (GCE) and screen-printed electrode (SPCE) modified with CQDs dispersion—drop casting                | Electrochemical sensor for dopamine, LOD = 0.099 $\mu\text{M}$   | [163]      |
|   | Electrochemical synthesis; two graphite rods were used as anode and cathode in mineral water (Wahaha water) as electrolyte  | ND <sup>1</sup><br>(500/558 nm)                        | GCE prepared by CQDs drop-casting on the electrode surface  | Photocatalytic activity for $\text{H}_2$ production, contaminant elimination activity at solid-solid interface           | [165]      |
| Graphite electrode                            | Electrochemical synthesis; graphite working electrode, platinum foil counter electrode and Ag/AgCl reference electrode in EtOH/NaOH electrolyte, applied voltage 5 V for 3 h in nitrogen atmosphere | 4.6–11.2%<br>(365/436–438 nm)                          | -   | Determination of $\text{Fe}^{3+}$ ion in tap water (LOD = 1.8 $\mu\text{M}$ ) by measuring PL intensity and cell imaging | [29]       |
|   | Electrochemical synthesis; electrooxidation of graphite column electrode at 3 V in 0.1 M $\text{KH}_2\text{PO}_4$   | ND <sup>1</sup><br>(ND <sup>1</sup> )                  | CQDs incorporated in PANI <sup>2</sup> , photo-assisted cyclic voltammetry electrodeposition                                | All-solid-state flexible supercapacitor  | [166]      |
| Amino acids<br>(Cys, Asp, Ser, Met, His, Arg) | Electrochemical synthesis; Pt working and auxiliary electrode and Ag/AgCl reference electrode, potential range from 1 V to 10 V   | 46.2–Asp<br>(360/430 nm)                               | -   | Cell imaging, fiber staining, and sensitive detection of $\text{Fe}^{3+}$ ions (LOD = 0.5 $\mu\text{M}$ )                | [167]      |
| Carbon rod                                    | Electrochemical synthesis; two carbon rods were used as anode and cathode in ultrapure water, constant voltage of 50 V was applied, electrolyte was stirred for 96 h                                | ND <sup>1</sup><br>(ND <sup>1</sup> )                  | Screen-printed electrode (SPCE) modified with CQDs dispersion—drop casting; dried in oven at 90 $^\circ\text{C}$ for 10 min | Electrochemical sensor for ferric ions ( $\text{Fe}^{3+}$ ), LOD = 0.44 $\pm$ 0.04 ppm                                   | [168]      |

<sup>1</sup> ND—no data presented, <sup>2</sup> PANI—polyaniline.

The study of electrochemical synthesis of CQDs by exfoliating graphite rods in electrolyte that consisted of two ionic liquids and a water mixture with an applied voltage of 15 V was reported by Li et al. [164]. The size of the obtained CDs has varied with the fraction of water in the mixed electrolyte (it decreased with the increase of water fraction). The smallest CQDs of the average size of 3.1 nm were obtained when the water fraction in the mixed electrolyte was 65%. The surface characterization of CQDs with FTIR and XPS has shown that prepared nanoparticles have many –OH functional groups on their surface, which have improved their solubility. The CQDs have been used in cell labeling and bacteria labeling *in vitro* conditions. In addition, electrochemical synthesis of carbon quantum dots (CQDs) by using a graphite rod was also reported by Devi et al. [163]. The graphite rod (width approximately 0.2 cm) was used as the anode and cathode in the alkaline 0.1 M NaOH/EtOH/water electrolyte. The applied constant current of 50 mA was used to start electrochemical exfoliation of the anode and the generation of CQDs. They have proposed the following mechanism of CQD synthesis: the first step includes the formation of sodium salt of ethanol ( $C_2H_5ONa$ ) and the hydroxide ions ( $OH^-$ ) in the electrolyte solution. In the next step,  $OH^-$  ions were attracted to the anode, which has started to oxidize, and the electrochemical cutting of graphite led to the formation of CQDs. The particle sizes of the obtained CQDs were measured with UV/Vis spectroscopy and high-resolution transmission electron microscopy (HR-TEM), while the lattice structure and functional groups were analyzed with XRD and FTIR spectroscopy. The dispersion of CQDs was used to modify the surface of glassy carbon electrode (GCE) and screen-printed carbon electrode (SPCE) by the drop-casting method (10  $\mu$ L of dispersion was put on the clean electrode surface and dried at room temperature for 10 min). The authors have selected the SPCE/CQD electrode as an electrochemical sensor for dopamine detection in phosphate buffer pH = 7.4. A Nafion (Nf) layer was coated on the SPCE/CQD sensor to avoid interferences with ascorbic acid in phosphate buffer. The calibration curve for dopamine was recorded in the 1–7  $\mu$ M region, and the limit of detection was calculated to be  $LOD = 0.099 \mu$ M. The prepared CQDs have shown electrocatalytic activity, which can be attributed to their negatively charged functional groups ( $OH^-$ ,  $COO^-$ ), which attracted positively charged dopamine in phosphate buffer pH = 7.4. The SPCE/CQD sensor was also used for the detection of dopamine in spiked human urine samples with acceptable recovery values (recovery values varied from 103 to 105%).

Furthermore, Li et al. [164] performed the electrochemical synthesis of CQDs in a three-electrode system, which consisted of a working graphite electrode, platinum foil as the counter electrode, and Ag/AgCl as the reference electrode in NaOH/EtOH electrolyte for the detection of  $Fe^{3+}$  ions. The potentiostatic voltage of 5 V was applied to the graphite working electrode for 3 h in  $N_2$  atmosphere to obtain CQDs. The average diameter of CQDs was determined to be  $4.0 \pm 0.2$ , showing high crystallinity. During the synthesis and storage of CQDs, dispersion was colorless, while the color gradually changed to bright yellow when dispersion was stored at room temperature due to the oxygenation of their surfaces. They were used in the detection of  $Fe^{3+}$  ions at pH = 6.0 in a concentration range from 10 to 200  $\mu$ M, while the LOD was determined as  $LOD = 1.8 \mu$ M. Furthermore, the applicability of CQDs for the detection of  $Fe^{3+}$  ions in tap water and for cell imaging of bamboo fiber cells was determined. Another interesting example for the detection of  $Fe^{3+}$  ions from versatile N-CQDs obtained by electrochemical synthesis was proposed by Niu et al. [167]. The electrochemical approach was employed for the production of N-doped carbon quantum dots (N-CQDs) using different amino acids (L-cysteine (Cys), L-aspartic acid (Asp), L-serine (Ser), L-methionine (Met), L-histidine (His), and L-arginine (Arg)) as the green precursors in N-CQDs synthesis in a three-electrode system (Pt sheets as the working and auxiliary electrodes and Ag/AgCl as the reference electrode in electrolyte 3 M  $NH_3 \times H_2O$  in ultrapure water). The obtained N-CQDs were water dispersible, and they showed strong photoluminescence and stable electrochemiluminescent properties. Aspartic acid-based N-CQDs (Asp-N-CQDs) have shown higher quantum yield com-

pared to N-CQDs obtained from other amino acids under the same electrochemical conditions. The N-CQDs were well dispersed in aqueous medium with uniform morphology and an average size of  $2.95 \pm 0.12$  nm as determined by TEM. The excellent photoluminescence, high stability, and low cytotoxicity of the Asp-N-CQDs enabled their applications in cell imaging, fiber staining, and sensitive detection of  $\text{Fe}^{3+}$  ions at pH = 6.0, in the linear range from 2 to 600  $\mu\text{M}$  with LOD = 0.5  $\mu\text{M}$ . The application of CQDs composite for the purposes of energy storage was purposed by Zhao et al. [166]. A new composite electrode material consisting of carbon quantum dots–polyaniline/carbon fibers (CQDs-PANI/CFs) was fabricated by directly photoelectrodepositing the CQDs and PANI on the surface of CFs. The CQDs were interconnected with PANI to promote electrons transportation, which could efficiently improve the conductivity of PANI and enhance its faradic process. The CQDs were prepared with the electrooxidation of a graphite column electrode at 3.0 V with a reference saturated calomel electrode and Pt counter electrode in 0.1 M  $\text{KH}_2\text{PO}_4$  electrolyte. The CQDs-PANI supercapacitor exhibits a specific capacitance of 169.2  $\text{mFcm}^2$ , an energy density of 33.8  $\text{mWhcm}^2$ , and a power density of 0.3  $\text{mWcm}^2$  at a current density of 1.0  $\text{mAcm}^2$ . The authors have shown that a CQDs-PANI hybrid can be used as an electrode material for flexible energy storage devices.

Although there are many examples reporting the electrochemical synthesis of carbon dots, the application of CQDs is also found in electrochemical sensing, most commonly by the electrode modification with CQDs for the sensitive and selective response toward target molecules. Several interesting examples of the application of CQDs in electrochemical sensing are listed in Table 8.

**Table 8.** Selected CQDs for the applications in electrochemical sensing.

| Precursor            | Preparation of CQDs   | Modification Method (CQDs/Electrode)  | Applications  | References |
|----------------------|---|---|---|------------|
| Citric acid          | Solvothermal bottom-up synthesis  | CQD–polypyrrole composite   | Supercapacitor electrode material   | [42]       |
|                      | Pyrolysis; temperature of 300 °C for 3 h under nitrogen flow  | PVP <sup>1</sup> ; GCE modified with CQDs capped with PVP   | Electrochemical sensor for etoposide (ETO), LOD = 5 nm, determination of ETO in real samples under optimal conditions | [43]       |
| Citric acid and urea | Microwave-assisted method   |   |   |            |
| Sucrose              | Hydrothermal synthesis; sucrose, and NaOH in a Teflon-lined stainless-steel autoclave at 160 °C for 4 h | Carbon paste electrode modified with nitrogen-doped CQDs  | Electrochemical sensor for TOBRA <sup>2</sup> , LOD = 3.2 nM  | [169]      |
| Graphite             | Green modification of Hummers method  | Glassy carbon electrode modified with CQDs, 40 $\mu\text{L}$ of suspension ( $\gamma = 1 \text{ mg mL}^{-1}$ ) placed on the electrode surface and dried at 40 °C for 1 h | Electrochemical sensor for dopamine (LOD = 2.7 $\mu\text{M}$ ) and uric acid (LOD = 1.3 $\mu\text{M}$ )               | [170]      |
| Salmon DNA           | Hydrothermal/DNA hydrogel   | Drop-casting sol on ITO plate   | Dopamine detection<br>LOD = 5 $\mu\text{M}$   | [171]      |
| Carbon soot          | Mixed with NaOH, followed by centrifugation and multiple sonication                                     | Carbon paste prepared by CQDs drop casting on the electrode surface   | Electrochemical sensor for adrenaline, LOD = 6 nM   | [172]      |

|         |  |   |   |       |
|---------|--|---|---|-------|
| Glucose | Microwave synthesis; glucose mixes with PEG-200 <sup>3</sup> | GCE modified with CQDs with electropolymerization (cyclic voltammetry, 20 cycles, -1 to 2 V, scan rate 50 mV/s) | Electrochemical sensor for ascorbic acid (AA), LOD = 10 $\mu$ M | [173] |
|---------|--|---|---|-------|

<sup>1</sup> PVP—polyvinylpyrrolidone; <sup>2</sup> TOBRA—tobramycin sulfate; <sup>3</sup> PEG-200—polyethylene glycol 200.

Furthermore, Mittal et al. [42] used a solvothermal “bottom-up” approach for CQDs synthesis by using citric acid as a carbon precursor. The obtained CQDs were incorporated in a polypyrrole matrix by their dispersion during the in situ polymerization of pyrrole. The obtained CQD–polypyrrole composite was used as a supercapacitor electrode material. The electrochemical properties of the CQD–polypyrrole composite were studied with cyclic voltammetry and galvanostatic charge–discharge studies. Cyclic voltammetry has shown that the incorporation of CQDs in a polypyrrole matrix has enhanced the electrochemical properties of polypyrrole. The composite had 33% higher specific capacitance compared to neat polypyrrole, which can be explained with the interfacial charge transfer between CQDs and the polypyrrole matrix. Moreover, citric acid and urea were used for obtaining N-CQDs by microwave-assisted synthesis, while second CQDs were prepared by hydrothermal treatment of the mixture of sucrose and NaOH in the study reported by Fares et al. [169]. The schematic illustration of the bare CQDs and CQDs/CPE preparation is shown in Figure 7. The N-CQDs obtained with the microwave-assisted method had a smaller particle size (less than 10 nm) and higher monodispersity with no apparent by-products compared to hydrothermally obtained CQDs, and therefore, N-CQDs were used for bare carbon paste electrode modification.

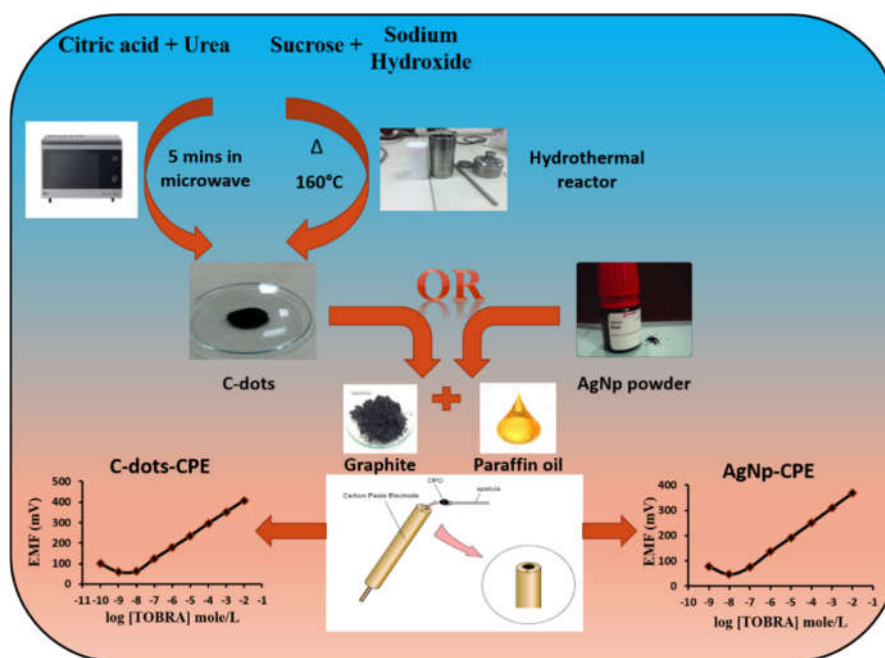


**Figure 7.** Schematic illustration of the preparation of N-CQDs by a microwave-assisted method. Carbon paste electrode was modified with N-CQDs for the potentiometric determination of tobramycin sulfate in pharmaceutical formulation and spiked human plasma [169].

The modified electrode was used for the potentiometric determination of tobramycin sulfate (TOBRA) in pharmaceutical formulation and spiked human plasma. It was determined that the addition of CQDs in carbon paste has significantly improved the perfor-

mance of the electrode (LOD was 3.2 nM, linear dynamic response was in a wide concentration range from  $10^{-8}$  M to  $10^{-2}$  M and the electrode selectivity was improved). A design of a CQDs-modified carbon paste electrode sensor for the selective detection of the hormone adrenaline was proposed by Sharath Shankar et al. [172]. Carbon soot was used as a carbon precursor in CQDs synthesis. The obtained CQDs were used to modify carbon paste electrode (CPE). The obtained CQDs/CPE sensor was used for the determination of adrenaline (AD). The sensing mechanism was suggested based on the presence of the hydroxyl groups on the CQDs surface. It is known that adrenaline exists in the cationic form, and electrostatic attraction between negatively charged hydroxyl groups and positively charged adrenaline could produce a redox current (Figure 8). The sensor had a lower limit of detection of 6 nM, which showed that CQDs have increased the sensitivity of the sensor. The selectivity of the modified electrode was also improved, since the simultaneous determination of adrenaline (AD), ascorbic acid (AA), and serotonin (5-HT) were enabled, as the overlapping peaks on the carbon paste electrode were resolved to three peaks on the modified CQDs/CPE. The adrenaline concentration was also determined in real samples (injection sample of adrenaline bitartrate). Wei et al. [173] performed a microwave-assisted synthesis of CQDs by using glucose as a precursor. The obtained CQDs were used for glassy carbon electrode modification with electropolymerization (20 cycles,  $\nu = 50$  mV/s, potential range from  $-1.0$  to  $2.0$  V). The obtained sensor was used for the determination of ascorbic acid (AA), and it was investigated by cyclic voltammetry (CV), electrochemical impedance spectroscopy (EIS), and differential pulse voltammetry (DPV). It was determined that the sensor has two linear ranges ( $0.01$ – $3$  mM and  $4$ – $12$  mM). A low limit of detection was determined as  $\text{LOD} = 10$  nM. The high sensor sensitivity in both linear ranges was observed. In addition, the selectivity of the sensor was also satisfactory, which enabled the determination of AA in the presence of dopamine (DA) and uric acid (UA).

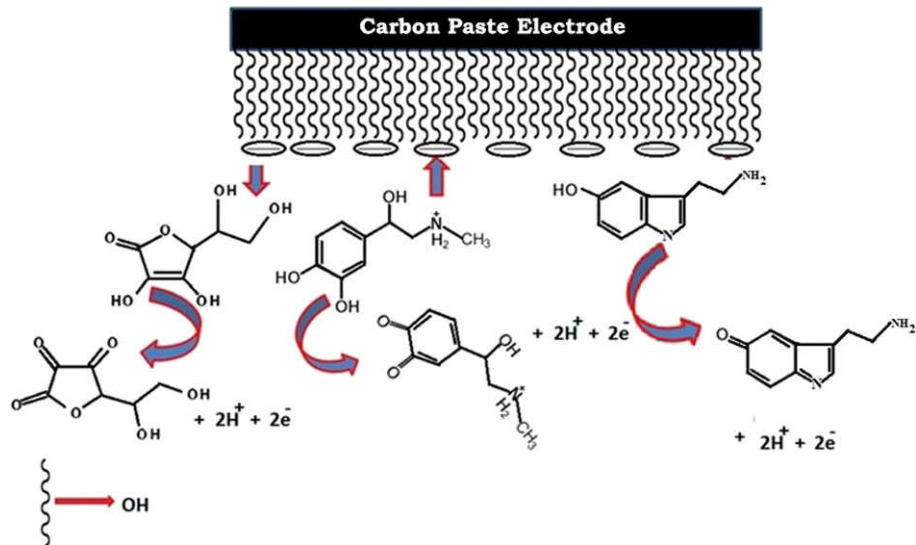


**Figure 8.** Mechanism of sensing and oxidation of ascorbic acid (AA), adrenaline (AD), and serotonin (5-HT) on CQDs/carbon paste electrode (CPE) [172].

In addition, CQDs have been used in the preparation of supercapacitor electrode material and for the electrode modification [42,166]. It was determined that CQDs have improved electrochemical properties of the supercapacitor electrode material and performance of the modified electrodes (the increase in sensor selectivity and sensitivity and decrease in LOD of the modified electrodes were observed). The use of the developed sensors in the simultaneous determination of several analytes was also enabled.

In summary, compared to other synthesis methods of CQDs (solvothermal, microwave-assisted, and hydrothermal synthesis) which often require complex procedures,

very high temperatures, extensive acid usage, and could be the cause of more chemical waste generation, the electrochemical synthesis of CQDs (especially exfoliation of graphite) represents a green method of synthesis that can be performed relatively fast at room temperature with a high product yield. The main advantages of electrochemical synthesis of CQDs are mild reaction conditions, simple instrumentation, possibility of using low-cost carbon precursors/electrodes, and satisfactory product yield. The obtained CQDs are of high quality; sometimes, the particle size can be adjusted by varying the applied potential, showing also good fluorescence behavior without complicated purification and passivation procedures applied.

## 8. Conclusions and Future Outlooks

Carbon quantum dots (CQDs) have emerged as a promising tool in biosensing, bioimaging, and drug and gene delivery. Small-sized, nanostructured fluorophores with an average size below 10 nm have received increasing attention due to their remarkable properties, primarily for the fluorescence emission, photo and chemical stability, water solubility, and biocompatibility, with relatively versatile possibilities of synthesis and surface modifications or heteroatom doping. The main focus of this paper is a comprehensive review of the recent developments in CQDs preparation and modification toward designing sensitive and highly selective sensors for target analyte detection. In addition, special emphasis has been placed on the utilization of biomass and waste as an inexpensive and renewable carbon source toward obtaining highly efficient CQDs, at the same time producing highly valuable products and also reducing the impact on the environment. This green approach could be also useful for the cost reduction of sensors/biosensors, by choosing low-cost carbon sources for sensing material fabrication as an efficient alternative to expensive and often toxic metal precursors. Carbon dots have been extensively studied for the theranostic and (bio)sensing purposes. The sensitivity and selectivity of the designed sensors are strongly dependent on the surface functionalization, used carbon precursors, and operating conditions in CQDs preparation. In this review, recent developments in the preparation and application of CQDs have been presented with an emphasis on the studies reported in the last five years. Although the efficient and superior performance of versatile CQDs in sensing has been presented in this work, there are still some challenges to overcome in the future for better sensing efficiency: (i) product yield is still very low in producing highly purified CQDs, which limits the large-scale production of CQDs; (ii) the proper selection of synthetic technique is essential toward obtaining uniformed and small-sized particles often affecting chemical, structural, and optical properties; (iii) the real sample analysis, often representing a complex system, contains various ions and complex molecules that could interfere with the target analyte or it could cause damage on the sensor, and (iv) the PL response of CQDs is usually unstable in acidic environments, hence limiting their application in environmental analysis and metal ion sensing in real systems. The optimal performance of CQDs as sensory materials could be evaluated in terms of high selectivity and sensitivity, long-term stability, biocompatibility, and large specific active area. The selectivity and sensitivity could be also improved by introducing metal nanoparticles to CQDs (most commonly, silver and gold nanoparticles). As the metal–CQDs nanocomposite is assembled, fluorescence quenching is observed. The binding of target analyte causes the recovery of the fluorescence emission intensity, and this phenomenon could be also achieved by aptamer-based biosensors. Regarding the application in bioimaging and cell sensing, the main issue represents the low tissue penetration and toxicity for biological systems of the short-wavelength light. An NIR light is preferably used for deep-tissue bioimaging, presenting a promising research direction in cellular sensing and imaging. In these challenging times in dealing with SARS-CoV-2 (COVID-19), the investigation of a novel antiviral agent is certainly of interest, as well as the rapid, low-cost, and accurate detection of COVID-19. A possible direction of further investigation could include the coupling CQDs and the existing therapeutic molecules or

other biomolecules useful in battling the COVID-19 virus, either for biosensing or for the therapeutic purposes of COVID-19 treatment.

**Author Contributions:** S.Š., D.G.; writing—original draft preparation, S.J., A.S., M.M.-K., T.M. I.J.; writing—review and editing, S.J., I.J.; funding acquisition and review. All authors have read and agreed to the published version of the manuscript.

**Funding:** This research was funded by Croatian Science Foundation under the project UIP-2017-05-9909.

**Institutional Review Board Statement:** Not applicable.

**Informed Consent Statement:** Not applicable.

**Data Availability Statement:** Not applicable.

**Acknowledgments:** This work has been supported by Croatian Science Foundation under the project “Application of innovative techniques of the extraction of bioactive compounds from by-products of plant origin” (UIP-2017-05-9909).

**Conflicts of Interest:** The authors declare no conflict of interest.

## References

1. Rauti, R.; Musto, M.; Bosi, S.; Prato, M.; Ballerini, L. Properties and behavior of carbon nanomaterials when interfacing neuronal cells: How far have we come? *Carbon* **2019**, *143*, 430–446, doi:10.1016/j.carbon.2018.11.026.
2. Meng, W.; Bai, X.; Boyang, W.; Zhongyi, L.; Lu, S.; Yang, B. Biomass-Derived Carbon Dots and Their Applications. *Energy Environ. Mat. C* **2019**, *2*, 172–192, doi:10.1002/eem2.12038.
3. Iravani, S.; Varma, R.S. Green synthesis, biomedical and biotechnological applications of carbon and graphene quantum dots. A review. *Environ. Chem. Lett.* **2020**, *18*, 703–727, doi:10.1007/s10311-020-00984-0.
4. Shankar, S.; Ramachandran, V.; Raj, R.P.; Tv, S.; Kumar, S. Carbon Quantum Dots: A Potential Candidate for Diagnostic and Therapeutic Application. In *Nanobiomaterial Engineering*, 1st ed.; Chandra, P., Prakash, R., Eds.; Springer Nature Singapore: Singapore, 2020; pp. 47–90, doi:10.1007/978-981-32-9840-8\_3.
5. Ghosh, D.; Sarkar, K.; Devi, P.; Kim, K.H.; Kumara, P. Current and future perspectives of carbon and graphene quantum dots: From synthesis to strategy for building optoelectronic and energy devices. *Renew. Sust. Energ. Rev.* **2021**, *135*, 110391, doi:10.1016/j.rser.2020.110391.
6. Xu, X.; Ray, R.; Gu, Y.; Ploehn, H.J.; Gearheart, L.; Raker, K.; Scrivens, W.A. Electrophoretic Analysis and Purification of Fluorescent Single-Walled Carbon Nanotube Fragments. *J. Am. Chem. Soc.* **2004**, *126*, 12736–12737, doi:10.1021/ja040082h.
7. Sun, Y.P.; Zhou, B.; Lin, Y.; Wang, W.; Fernando, K.S.; Pathak, P.; Mezziani, M.J.; Harruff, B.A.; Wang, X.; Wang, H.; et al. Quantum-sized carbon dots for bright and colorful photoluminescence. *J. Am. Chem. Soc.* **2006**, *128*, 7756–7757, doi:10.1021/ja062677d.
8. Su, W.; Wu, H.; Xu, H.; Zhang, Y.; Li, Y.; Li, X.; Fan, L. Carbon dots: A booming material for biomedical applications. *Mater. Chem. Front.* **2020**, *4*, 821–836, doi:10.1039/C9QM00658C.
9. Molaei, M.J. Carbon quantum dots and their biomedical and therapeutic applications: A review. *RSC Adv.* **2019**, *9*, 6460–6481, doi:10.1039/C8RA08088G.
10. Li, M.; Chen, T.; Gooding, J.J.; Liu, J. Review of Carbon and Graphene Quantum Dots for Sensing. *ACS Sens.* **2019**, *4*, 1732–1748, doi:10.1021/acssensors.9b00514.
11. Nair, A.; Haponiuk, J.T.; Thomas, S.; Gopi, S. Natural carbon-based quantum dots and their applications in drug delivery: A review. *Biomed. Pharmacother.* **2020**, *132*, 110834, doi:10.1016/j.biopha.2020.110834.
12. Rastogi, A.; Pandey, F.; Parmar, A.; Singh, S.; Hegde, G.; Manohar, R. Effect of carbonaceous oil palm leaf quantum dot dispersion in nematic liquid crystal on zeta potential, optical texture and dielectric properties. *J. Nanostruct. Chem.* **2021**, doi:10.1007/s40097-020-00382-6.
13. Devi, P.; Rajput, P.; Thakur, A.; Kim, K.; Kumar, P. Recent advances in carbon quantum dot-based sensing of heavy metals in water. *TrAC* **2019**, *114*, 171–195, doi:10.1016/j.trac.2019.03.003.
14. Gao, X.; Du, C.; Zhuang, Z.; Chen, W. Carbon quantum dot-based nanoprobe for metal ion detection. *J. Mater. Chem. C* **2016**, *4*, 6927–6945, doi:10.1039/C6TC02055K.
15. Yoo, D.; Park, Y.; Cheon, B.; Park, M. Carbon Dots as an Effective Fluorescent Sensing Platform for Metal Ion Detection. *Nanoscale Res. Lett.* **2019**, *14*, 272, doi:10.1186/s11671-019-3088-6.
16. Qu, D.; Wang, X.; Bao, Y.; Sun, Z. Recent advance of carbon dots in bio-related applications. *J. Phys. Mater.* **2020**, *3*, 022003, doi:10.1088/2515-7639/ab7cb9.
17. Devi, P.; Saini, S.; Kim, K.H. The advanced role of carbon quantum dots in nanomedical applications. *Biosens. Bioelectron.* **2019**, *141*, 111158, doi:10.1016/j.bios.2019.02.059.
18. Cui, L.; Ren, X.; Wang, J.; Sun, M. Synthesis of homogeneous carbon quantum dots by ultrafast dual-beam pulsed laser ablation for bioimaging. *Mater. Today Nano* **2020**, *2*, 100091, doi:10.1016/j.mtnano.2020.100091.

19. Zhang, Z.; Zheng, T.; Li, X.; Xu, J.; Zeng, H. Progress of Carbon Quantum Dots in Photocatalysis Applications. *Part. Part. Syst. Charact.* **2016**, *33*, 457–472, doi:10.1002/ppsc.201500243.
20. Tian, L.; Ghosh, D.; Chen, W.; Pradhan, S.; Chang, X.; Chen, S. Nanosized Carbon Particles from Natural Gas Soot. *Chem. Mater.* **2009**, *21*, 2803–2809, doi:10.1021/cm900709w.
21. Liu, R.; Wu, D.; Liu, S.; Koynov, K.; Knoll, W.; Li, Q. An Aqueous Route to Multicolor Photoluminescent Carbon Dots Using Silica Spheres as Carriers. *Angew. Chem.* **2009**, *48*, 4598–4601, doi:10.1002/anie.200900652.
22. Ray, S.C.; Saha, A.; Jana, N.R.; Sarkar, R. Fluorescent Carbon Nanoparticles: Synthesis, Characterization, and Bioimaging Application. *J. Phys. Chem. C* **2009**, *113*, 18546–18551, doi:10.1021/jp905912n.
23. Qiao, Z.A.; Wang, Y.; Gao, Y.; Li, H.; Dai, T.; Liua, Y.; Huo, Q. Commercially activated carbon as the source for producing multicolor photoluminescent carbon dots by chemical oxidation. *Chem. Commun.* **2010**, *46*, 8812–8814, doi:10.1039/C0CC02724C.
24. Deng, J.; Lu, Q.; Mi, N.; Li, H.; Liu, M.; Xu, M.; Tan, L.; Xie, Q.; Zhang, Y.; Yao, S. Electrochemical Synthesis of Carbon Nanodots Directly from Alcohols. *Chem. Eur. J.* **2014**, *20*, 4993–4999, doi:10.1002/chem.201304869.
25. Anwar, S.; Ding, H.; Xu, M.; Hu, X.; Li, Z.; Wang, J.; Liu, L.; Jiang, L.; Wang, D.; Dong, C.; et al. Recent Advances in Synthesis, Optical Properties, and Biomedical Applications of Carbon Dots. *ACS Appl. Bio. Mater.* **2019**, *2*, 2317–2338, doi:10.1021/acsabm.9b00112.
26. Pan, M.; Xie, X.; Liu, K.; Yang, J.; Hong, L.; Wang, S. Fluorescent Carbon Quantum Dots—Synthesis, Functionalization and Sensing Application in Food Analysis. *Nanomaterials* **2020**, *10*, 930, doi:10.3390/nano10050930.
27. Chen, Z.H.; Han, X.Y.; Lin, Z.Y.; Fan, Y.L.; Shi, G.; Zhang, S.; Zhang, M. Facile reflux synthesis of polyethyleneimine-capped fluorescent carbon dots for sequential bioassays toward Cu<sup>2+</sup>/H<sub>2</sub>S and its application for a logic system. *Biotechnol. Appl. Biochem.* **2019**, *66*, 426–433, doi:10.1002/bab.1739.
28. Wang, X.; Feng, Y.; Dong, P.; Huang, J. A Mini Review on Carbon Quantum Dots: Preparation, Properties, and Electrocatalytic Application. *Front. Chem.* **2019**, *7*, 671, doi:10.3389/fchem.2019.00671.
29. Liu, M.; Xu, Y.; Niu, F.; Gooding, J.J.; Liu, J. Carbon quantum dots directly generated from electrochemical oxidation of graphite electrodes in alkaline alcohols and the applications for specific ferric ion detection and cell imaging. *Analyst* **2016**, *141*, 2657–2664, doi:10.1039/c5an02231b.
30. Hou, Y.; Lu, Q.; Deng, J.; Li, H.; Zhang, Y. One-pot electrochemical synthesis of functionalized fluorescent carbon dots and their selective sensing for mercury ion. *Anal. Chim. Acta* **2015**, *866*, 69–74, doi:10.1016/j.aca.2015.01.039.
31. Farshbaf, M.; Davaran, S.; Rahimi, F.; Annabi, N.; Salehi, R.; Akbarzadeh, A. Carbon quantum dots: Recent progresses on synthesis, surface modification and applications. *Artif. Cells Nanomed. Biotechnol.* **2017**, *46*, 1331–1348, doi:10.1080/21691401.2017.1377725.
32. Shen, T.Y.; Jia, P.Y.; Chen, D.S.; Wang, L.N. Hydrothermal synthesis of N-doped carbon quantum dots and their application in ion-detection and cell-imaging. *Spectrochim. Acta A Mol. Biomol. Spectrosc.* **2021**, *248*, 119282, doi:10.1016/j.saa.2020.119282.
33. Crista, D.M.A.; Esteves da Silva, J.C.G.; Pinto da Silva, L. Evaluation of Different Bottom-up Routes for the Fabrication of Carbon Dots. *Nanomaterials* **2020**, *10*, 1316, doi:10.3390/nano10071316.
34. Chu, K.W.; Lee, S.L.; Chang, C.-H.; Liu, L. Recent Progress of Carbon Dot Precursors and Photocatalysis Applications. *Polymers* **2019**, *11*, 689, doi:10.3390/polym11040689.
35. Luo, J.; Sun, Z.; Zhou, W.; Mo, F.; Wu, Z.C.; Zhang, X. Hydrothermal synthesis of bright blue-emitting carbon dots for bioimaging and fluorescent determination of baicalein. *Opt. Mater.* **2021**, *113*, 110796, doi:10.1016/j.optmat.2020.110796.
36. Zheng, M.; Ruan, S.; Liu, S.; Sun, T.; Qu, D.; Zhao, H.; Xie, Z.; Gao, H.; Jing, X.; Sun, Z. Self-targeting fluorescent carbon dots for diagnosis of brain cancer cells. *ACS Nano* **2015**, *9*, 11455–11461, doi:10.1021/acsnano.5b05575.
37. Canevari, T.C.; Nakamura, M.; Cincotto, F.H.; de Melo, F.M.; Toma, H.E. High performance electrochemical sensors for dopamine and epinephrine using nanocrystalline carbon quantum dots obtained under controlled chronoamperometric conditions. *Electrochim. Acta* **2016**, *209*, 464–470, doi:10.1016/j.electacta.2016.05.108.
38. Eskalen, H.; Uruş, S.; Cömertpay, S.; Kurt, A.H.; Özgün, S. Microwave-assisted ultra-fast synthesis of carbon quantum dots from linter: Fluorescence cancer imaging and human cell growth inhibition properties. *Ind. Crop. Prod.* **2020**, *147*, 112209, doi:10.1016/j.indcrop.2020.112209.
39. Singh, R.K.; Kumar, R.; Singh, D.P.; Savu, R.; Moshkalev, S.A. Progress in microwave-assisted synthesis of quantum dots (graphene/carbon/semiconducting) for bioapplications: A review. *Mater. Today Chem.* **2019**, *12*, 282–314, doi:10.1016/j.mtchem.2019.03.001.
40. Wan, J.Y.; Yang, Z.; Liu, Z.G.; Wang, H.X. Ionic liquid-assisted thermal decomposition synthesis of carbon dots and graphene-like carbon sheets for optoelectronic application. *RSC Adv.* **2016**, *6*, 61292–61300, doi:10.1039/C6RA14181A.
41. Shang, W.; Cai, T.; Zhang, Y.; Liu, D.; Liu, S. Facile one pot pyrolysis synthesis of carbon quantum dots and graphene oxide nanomaterials: All carbon hybrids as eco-environmental lubricants for low friction and remarkable wear-resistance. *Tribol. Int.* **2018**, *118*, 373–380, doi:10.1016/j.triboint.2017.09.029.
42. Sagar Mittal, S.; Ramadas, G.; Vasanthmurali, N.; Madaneshwar, V.; Sathish Kumar, M.; Kothurkar, N. Carbon Quantum Dot-Polypyrrole Nanocomposite for Supercapacitor Electrodes. *IOP Conf. Ser. Mater. Sci. Eng.* **2019**, *577*, 012194, doi:10.1088/1757-899X/577/1/012194.
43. Nguyen, H.; Richtera, L.; Moulick, A.; Xhaxhiu, K.; Kudr, J.; Cernei, N.; Polanska, H.; Heger, Z.; Masarik, M.; Kopel, P.; et al. Electrochemical sensing of etoposide using carbon quantum dot modified glassy carbon electrode. *Analyst* **2016**, *141*, 2665–2675, doi:10.1039/C5AN02476E.

44. Kasprzyk, W.; Świergosz, T.; Bednarz, S.; Walas, K.; Bashmakova, N.V.; Bogdał, D. Luminescence phenomena of carbon dots derived from citric acid and urea—A molecular insight. *Nanoscale* **2018**, *10*, 13889–13894, doi:10.1039/C8NR03602K.
45. Baragau, I.A.; Power, N.P.; Morgan, D.J.; Lobo, R.A.; Roberts, C.S.; Titirici, M.M.; Middelkoop, V.; Diaz, A.; Dunn, S.; Kellici, S. Efficient Continuous Hydrothermal Flow Synthesis of Carbon Quantum Dots from a Targeted Biomass Precursor for On–Off Metal Ions Nanosensing. *ACS Sustain. Chem. Eng.* **2021**, *9*, 2559–2569, doi:10.1021/acssuschemeng.0c08594.
46. Qi, H.; Teng, M.; Liu, M.; Liu, S.; Li, J.; Yu, H.; Teng, C.; Huang, Z.; Liu, H.; Shao, Q.; et al. Biomass-derived nitrogen-doped carbon quantum dots: Highly selective fluorescent probe for detecting Fe<sup>3+</sup> ions and tetracyclines. *J. Colloid Interface Sci.* **2019**, *539*, 332–341, doi:10.1016/j.jcis.2018.12.047.
47. Yen, Y.T.; Lin, Y.S.; Chen, T.Y.; Chyueh, S.C.; Chang, H.T. Carbon dots functionalized papers for high-throughput sensing of 4-chloroethcathinone and its analogues in crime sites. *R. Soc. Open Sci.* **2019**, *6*, 191017, doi:10.1098/rsos.191017.
48. Achadu, O.J.; Lioe, D.X.; Kagawa, K.; Kawahito, S.; Park, E.Y. Fluoroimmunoassay of influenza virus using sulfur-doped graphitic carbon nitride quantum dots coupled with Ag<sub>2</sub>S nanocrystals. *Microchim. Acta* **2020**, *187*, 466, doi:10.1007/s00604-020-04433-1.
49. Kalaiyarasan, G.; Joseph, J.; Kumar, P. Phosphorus-Doped Carbon Quantum Dots as Fluorometric Probes for Iron Detection. *ACS Omega* **2020**, *5*, 22278–22288, doi:10.1021/acsomega.0c02627.
50. Yang, X.; Guo, Y.; Liang, S.; Hou, S.; Chu, T.; Ma, J.; Chen, X.; Zhou, J.; Suna, R. Preparation of sulfur-doped carbon quantum dots from lignin as a sensor to detect Sudan I in an acidic environment. *J. Mater. Chem. B* **2020**, *8*, 10788–10796, doi:10.1039/D0TB00125B.
51. Kou, X.; Jiang, S.; Park, S.J.; Meng, L.Y. A review: Recent advances in preparations and applications of heteroatom-doped carbon quantum dots. *Dalton Trans.* **2020**, *49*, 6915–6938, doi:10.1039/D0DT01004A.
52. Talwatkar, S.S.; Sunatkari, A.L.; Tamgadge, Y.S.; Pahurkar, V.G.; Muley, G.G. Surface passivation by L-arginine and enhanced optical properties of CdS quantum dots co-doped with Nd<sup>3+</sup>–Li<sup>+</sup>. *J. Nanostruct. Chem.* **2015**, *5*, 205–212, doi:10.1007/s40097-015-0151-4.
53. Lai, Z.; Guo, X.; Cheng, Z.; Ruan, G.; Du, F. Green Synthesis of Fluorescent Carbon Dots from Cherry Tomatoes for Highly Effective Detection of Trifluralin Herbicide in Soil Samples. *ChemistrySelect* **2020**, *5*, 1956–1960, doi:10.1002/slct.201904517.
54. Liu, W.; Li, C.; Sun, X.; Pan, W.; Yu, G.; Wang, J. Highly crystalline carbon dots from fresh tomato: UV emission and quantum confinement. *Nanotechnology* **2017**, *28*, 485705, doi:10.1088/1361-6528/aa900b.
55. Qiang, R.; Yang, S.; Hou, K.; Wang, J. Synthesis of carbon quantum dots with green luminescence from potato starch. *New J. Chem.* **2019**, *43*, 10826–10833, doi:10.1039/C9NJ02291K.
56. Su, R.; Wang, D.; Liu, M.; Yan, J.; Wang, J.; Zhan, Q.; Pu, Y.; Foster, N.R.; Chen, J.-F. Subgram-Scale Synthesis of Biomass Waste-Derived Fluorescent Carbon Dots in Subcritical Water for Bioimaging, Sensing, and Solid-State Patterning. *ACS Omega* **2018**, *3*, 13211–13218, doi:10.1021/acsomega.8b01919.
57. Tadesse, A.; Hagos, M.; RamaDevi, D.; Basavaiah, K.; Belachew, N. Fluorescent-Nitrogen-Doped Carbon Quantum Dots Derived from Citrus Lemon Juice: Green Synthesis, Mercury(II) Ion Sensing, and Live Cell Imaging. *ACS Omega* **2020**, *5*, 3889–3898, doi:10.1021/acsomega.9b03175.
58. Zhang, Q.; Liang, J.; Zhao, L.; Wang, Y.; Zheng, Y.; Wu, Y.; Jiang, L. Synthesis of Novel Fluorescent Carbon Quantum Dots from *Rosa roxburghii* for Rapid and Highly Selective Detection of *o*-nitrophenol and Cellular Imaging. *Front. Chem.* **2020**, *8*, 665, doi:10.3389/fchem.2020.00665.
59. Jin, H.; Gui, R.; Wang, Y.; Sun, J. Carrot-derived carbon dots modified with polyethyleneimine and Nile blue for ratiometric two-photon fluorescence turn-on sensing of sulfide anion in biological fluids. *Talanta* **2017**, *169*, 141–148, doi:10.1016/j.talanta.2017.03.083.
60. Ren, G.; Tang, M.; Chai, F.; Wu, H. One-Pot Synthesis of Highly Fluorescent Carbon Dots from Spinach and Multipurpose Applications. *Eur. J. Inorg. Chem.* **2018**, *2018*, 153–158, doi:10.1002/ejic.201701080.
61. Monte-Filho, S.S.; Andrade, S.I.E.; Lima, M.B.; Araujo, M.C.U. Synthesis of highly fluorescent carbon dots from lemon and onion juices for determination of riboflavin in multivitamin/mineral supplements. *J. Pharm. Anal.* **2019**, *9*, 209–216, doi:10.1016/j.jpha.2019.02.003.
62. Zulfajri, M.; Gedda, G.; Chang, C.J.; Chang, Y.P.; Huang, G.G. Cranberry Beans Derived Carbon Dots as a Potential Fluorescence Sensor for Selective Detection of Fe<sup>3+</sup> Ions in Aqueous Solution. *ACS Omega* **2019**, *4*, 15382–15392, doi:10.1021/acsomega.9b01333.
63. Ghosh, D.D.; Mukherjee, P.; Ghosh, D.; Banerjee, D. Carbon quantum dots prepared from onion extract as fluorescence turn-on probes for selective estimation of Zn<sup>2+</sup> in blood plasma. *Colloids Surf. A Physicochem. Eng. Asp.* **2021**, *61*, 125781, doi:10.1016/j.colsurfa.2020.125781.
64. Wang, C.; Shi, H.; Yang, M.; Yan, Y.; Liu, E.; Ji, Z.; Fan, J. Facile synthesis of novel carbon quantum dots from biomass waste for highly sensitive detection of iron ions. *Mater. Res. Bull.* **2020**, *124*, 110730, doi:10.1016/j.materresbull.2019.110730.
65. Tyagi, A.; Tripathi, K.; Singh, N.; Choudhary, S.; Gupta, R. Green synthesis of carbon quantum dots from lemon peel waste: Applications in sensing and photocatalysis. *RSC Adv.* **2016**, *6*, 72423–72432, doi:10.1039/C6RA10488F.
66. Su, A.; Wang, D.; Shu, X.; Zhong, Q.; Chen, Y.; Liu, J.; Wang, Y. Synthesis of Fluorescent Carbon Quantum Dots from Dried Lemon Peel for Determination of Carmine in Drinks. *Chem. Res. Chin. Univ.* **2018**, *34*, 164–168, doi:10.1007/s40242-018-7286-z.
67. Sun, X.; Liu, Y.; Niu, N.; Chen, L. Synthesis of molecularly imprinted fluorescent probe based on biomass-derived carbon quantum dots for detection of mesotrione. *Anal. Bioanal. Chem.* **2019**, *411*, 5519–5530, doi:10.1007/s00216-019-01930-y.

68. Bandi, R.; Gangapuram, B.R.; Dadigala, R.; Eslavath, R.; Singh, S.S.; Guttena, V. Facile and green synthesis of fluorescent carbon dots from onion waste and their potential applications as sensor and multicolour imaging agents. *RSC Adv.* **2016**, *6*, 28633–28639, doi:10.1039/C6RA01669C.
69. Vandarkuzhali, S.A.A.; Natarajan, S.; Jeyabalan, S.; Sivaraman, G.; Singaravadivel, S.; Muthusubramanian, S.; Viswanathan, B. Pineapple Peel-Derived Carbon Dots: Applications as Sensor, Molecular Keypad Lock, and Memory Device. *ACS Omega* **2018**, *3*, 12584–12592, doi:10.1021/acsomega.8b01146.
70. Srinivasan, V.; Jhonsi, M.A.; Kathiravan, A.; Ashokkumar, M. Fuel waste to fluorescent carbon dots and its multifarious applications. *Sens. Actuators B Chem.* **2019**, *282*, 972–983, doi:10.1016/j.snb.2018.11.144.
71. Boruah, A.; Saikia, M.; Das, T.; Goswamee, R.L.; Saikia, B.K. Blue-emitting fluorescent carbon quantum dots from waste biomass sources and their application in fluoride ion detection in water. *J. Photochem. Photobiol. B* **2020**, *209*, 111940, doi:10.1016/j.jphoto-biol.2020.111940.
72. Kang, C.; Huang, Y.; Yang, H.; Yan, X.F.; Chen, Z.P. A Review of Carbon Dots Produced from Biomass Wastes. *Nanomaterials* **2020**, *10*, 2316, doi:10.3390/nano10112316.
73. Carbonaro, C.M.; Corpino, R.; Salis, M.; Mocci, F.; Thakkar, S.V.; Olla, C.; Ricci, P.C. On the Emission Properties of Carbon Dots: Reviewing Data and Discussing Models. *J. Carbon Res.* **2019**, *5*, 60, doi:10.3390/c5040060.
74. Dimos, K. Carbon Quantum Dots: Surface Passivation and Functionalization. *Curr. Org. Chem.* **2016**, *20*, 682–695, doi:10.2174/1385272819666150730220948.
75. Koutsogiannis, P.; Thomou, E.; Stamatis, H.; Gournis, D.; Rudolf, P. Advances in fluorescent carbon dots for biomedical applications. *Adv. Phys. X* **2020**, *5*, 1758592, doi:10.1080/23746149.2020.1758592.
76. Edison, T.N.J.I.; Atchudan, R.; Sethuraman, M.G.; Shim, J.-J.; Lee, Y.R. Microwave assisted green synthesis of fluorescent N-doped carbon dots: Cytotoxicity and bio-imaging applications. *J. Photochem. Photobiol. B* **2016**, *161*, 154–161, doi:10.1016/j.jphoto-biol.2016.05.017.
77. Jing, S.; Zhao, Y.; Sun, R.; Zhong, L.; Peng, X.; Facile and High-Yield Synthesis of Carbon Quantum Dots from Biomass-Derived Carbons at Mild Condition. *ACS Sustain. Chem. Eng.* **2019**, *7*, 7833–7843, doi:10.1021/acssuschemeng.9b00027.
78. Lv, X.; Gao, C.; Han, T.; Shi, H.; Guo, W.; Improving the quantum yields of fluorophores by inhibiting twisted intramolecular charge transfer using electron-withdrawing group-functionalized piperidine auxochromes. *Chem. Commun.* **2020**, *56*, 715–718, doi:10.1039/C9CC09138F.
79. Zuo, P.; Lu, X.; Sun, Z.; Guo, Y.; He, H. A review on syntheses, properties, characterization and bioanalytical applications of fluorescent carbon dots. *Microchim. Acta* **2016**, *183*, 519–542, doi:10.1007/s00604-015-1705-3.
80. Huang, M.; Liang, X.; Zhang, Z.; Wang, J.; Fei, Y.; Ma, J.; Qu, S.; Mi, L. Carbon Dots for Intracellular pH Sensing with Fluorescence Lifetime Imaging Microscopy. *Nanomaterials* **2020**, *10*, 604, doi:10.3390/nano10040604.
81. Li, L.; Dong, T. Photoluminescence tuning in carbon dots: Surface passivation or/and functionalization, heteroatom doping. *J. Mater. Chem. C* **2018**, *6*, 7944–7970, doi:10.1039/C7TC05878K.
82. Li, P.; Li, S.F.Y. Recent advances in fluorescence probes based on carbon dots for sensing and speciation of heavy metals. *Nanophotonics* **2021**, *10*, 877–908, doi:10.1515/nanoph-2020-0507.
83. Zu, F.; Yan, F.; Bai, Z.; Xu, J.; Wang, Y.; Huang, Y.; Zhou, X. The quenching of the fluorescence of carbon dots: A review on mechanisms and applications. *Microchim. Acta* **2017**, *184*, 1899–1914, doi:10.1007/s00604-017-2318-9.
84. Miao, S.; Liang, K.; Kong, B. Förster resonance energy transfer (FRET) paired carbon dot-based complex nanoprobe: Versatile platforms for sensing and imaging applications. *Mater. Chem. Front.* **2020**, *4*, 128–139, doi:10.1039/C9QM00538B.
85. Briffa, J.; Sinagra, E.; Blundell, R. Heavy metal pollution in the environment and their toxicological effects on humans. *Heliyon* **2020**, *6*, e04691, doi:10.1016/j.heliyon.2020.e04691.
86. Issa, M.A.; Abidin, Z.Z.; Sobri, S.; Rashid, S.A.; Mahdi, M.A.; Ibrahim, N.A. Fluorescent recognition of Fe<sup>3+</sup> in acidic environment by enhanced-quantum yield N-doped carbon dots: Optimization of variables using central composite design. *Sci. Rep.* **2020**, *10*, 11710, doi:10.1038/s41598-020-68390-8.
87. Yang, G.; Wan, X.; Su, Y.; Zenga, X.; Tang, J. Acidophilic S-doped carbon quantum dots derived from cellulose fibers and their fluorescence sensing performance for metal ions in an extremely strong acid environment. *J. Mater. Chem. A* **2016**, *4*, 12841–12849, doi:10.1039/C6TA05943K.
88. Liu, L.; Zhang, S.; Zheng, X.; Li, H.; Chen, Q.; Qin, K.; Dinga, Y.; Wei, Y. Carbon dots derived from *Fusobacterium nucleatum* for intracellular determination of Fe<sup>3+</sup> and bioimaging both in vitro and in vivo. *Anal. Methods* **2021**, *13*, 1121–1131, doi:10.1039/D1AY00020A.
89. Chen, Y.; Sun, X.; Pan, W.; Yu, G.; Wang, J. Fe<sup>3+</sup>-Sensitive Carbon Dots for Detection of Fe<sup>3+</sup> in Aqueous Solution and Intracellular Imaging of Fe<sup>3+</sup> Inside Fungal Cells. *Front. Chem.* **2020**, *7*, 911, doi:10.3389/fchem.2019.00911.
90. Pu, Z.F.; Wen, Q.L.; Yang, Y.J.; Cui, X.M.; Ling, J.; Liu, P.; Cao, Q.E. Fluorescent carbon quantum dots synthesized using phenylalanine and citric acid for selective detection of Fe<sup>3+</sup> ions. *Spectrochim. Acta A Mol. Biomol. Spectrosc.* **2020**, *15*, 117944, doi:10.1016/j.saa.2019.117944.
91. Mohammed, L.J.; Omer, K.M. Dual functional highly luminescence B, N Co-doped carbon nanodots as nanothermometer and Fe<sup>3+</sup>/Fe<sup>2+</sup> sensor. *Sci. Rep.* **2020**, *10*, 3028, doi:10.1038/s41598-020-59958-5.
92. Yu, J.; Xu, C.; Tian, Z.; Lina, Y.; Shia, Z. Facilely synthesized N-doped carbon quantum dots with high fluorescent yield for sensing Fe<sup>3+</sup>. *New J. Chem.* **2016**, *40*, 2083–2088, doi:10.1039/C5NJ03252K.

93. Wu, P.; Li, W.; Wu, Q.; Liu, Y.; Liu, S. Hydrothermal synthesis of nitrogen-doped carbon quantum dots from microcrystalline cellulose for the detection of Fe<sup>3+</sup> ions in an acidic environment. *RSC Adv.* **2017**, *7*, 44144–44153, doi:10.1039/C7RA08400E.
94. Wu, H.; Jiang, J.; Gu, X.; Tong, C. Nitrogen and sulfur co-doped carbon quantum dots for highly selective and sensitive fluorescent detection of Fe(III) ions and L-cysteine. *Microchim. Acta* **2017**, *184*, 2291–2298, doi:10.1007/s00604-017-2201-8.
95. Deng, X.; Feng, Y.; Li, H.; Du, Z.; Teng, Q.; Wang, H. N-doped carbon quantum dots as fluorescent probes for highly selective and sensitive detection of Fe<sup>3+</sup> ions. *Particuology* **2018**, *41*, 94–100, doi:10.1016/j.partic.2017.12.009.
96. Lu, M.; Duan, Y.; Song, Y.; Tan, J.; Zhou, L. Green preparation of versatile nitrogen-doped carbon quantum dots from watermelon juice for cell imaging, detection of Fe<sup>3+</sup> ions and cysteine, and optical thermometry. *J. Mol. Liquids* **2018**, *269*, 766–774, doi:10.1016/j.molliq.2018.08.101.
97. Kwonbeen, K.; Jongsung, K. Synthesis of Carbon Quantum Dots from Jujubes for Detection of Iron(III) Ions. *J. Nanosci. Nanotechnol.* **2018**, *18*, 1320–1322, doi:10.1166/jnn.2018.14901.
98. Jiang, X.; Shi, Y.; Liu, X.; Wang, M.; Song, P.; Xu, F.; Zhang, X. Synthesis of Nitrogen-Doped Lignin/DES Carbon Quantum Dots as a Fluorescent Probe for the Detection of Fe<sup>3+</sup> Ions. *Polymers* **2018**, *10*, 1282, doi:10.3390/polym10111282.
99. Shi, B.; Su, Y.; Zhang, L.; Huang, M.; Liu, R.; Zhao, S. Nitrogen and Phosphorus Co-Doped Carbon Nanodots as a Novel Fluorescent Probe for Highly Sensitive Detection of Fe<sup>3+</sup> in Human Serum and Living Cells. *ACS Appl. Mater. Interfaces* **2016**, *8*, 10717–10725, doi:10.1021/acsami.6b01325.
100. Zhu, J.; Chu, H.; Wang, T.; Wang, C.; Wei, Y. Fluorescent probe based nitrogen doped carbon quantum dots with solid-state fluorescence for the detection of Hg<sup>2+</sup> and Fe<sup>3+</sup> in aqueous solution. *Microchem. J.* **2020**, *158*, 105142, doi:10.1016/j.microc.2020.105142.
101. Huang, H.; Ge, H.; Ren, Z.; Huang, Z.; Xu, M.; Wang, X. Controllable Synthesis of Biocompatible Fluorescent Carbon Dots from Cellulose Hydrogel for the Specific Detection of Hg<sup>2+</sup>. *Front. Bioeng. Biotechnol.* **2021**, *9*, 617097, doi:10.3389/fbioe.2021.617097.
102. Chen, Y.; Sun, X.; Wang, X.; Pan, W.; Yu, G.; Wang, J. Carbon dots with red emission for bioimaging of fungal cells and detecting Hg<sup>2+</sup> and ziram in aqueous solution. *Spectrochim. Acta A Mol. Biomol. Spectrosc.* **2020**, *233*, 118230, doi:10.1016/j.saa.2020.118230.
103. Guo, Y.; Zhang, L.; Cao, F.; Leng, Y. Thermal treatment of hair for the synthesis of sustainable carbon quantum dots and the applications for sensing Hg<sup>2+</sup>. *Sci. Rep.* **2016**, *6*, 35795, doi:10.1038/srep35795.
104. Tang, W.; Wang, Y.; Wang, P.; Di, J.; Yang, J.; Wu, Y. Synthesis of strongly fluorescent carbon quantum dots modified with polyamidoamine and a triethoxysilane as quenchable fluorescent probes for mercury(II). *Microchim. Acta* **2016**, *183*, 2571–2578, doi:10.1007/s00604-016-1898-0.
105. Wan, X.; Li, S.; Zhuang, L.; Tang, J. L-Tryptophan-capped carbon quantum dots for the sensitive and selective fluorescence detection of mercury ion in aqueous solution. *J. Nanopart. Res.* **2016**, *18*, 202, doi:10.1007/s11051-016-3441-y.
106. Huang, H.; Weng, Y.; Zheng, L.; Yao, B.; Weng, W.; Lin, X. Nitrogen-doped carbon quantum dots as fluorescent probe for “off-on” detection of mercury ions, L-cysteine and iodide ions. *J. Colloid Interface Sci.* **2017**, *506*, 373–378, doi:10.1016/j.jcis.2017.07.076.
107. Liu, T.; Xue Dong, J.; Liu, G.S.; Li, N.; Lin, M.S.; Fan, Y.Z.; Lei, J.L.; Luo, H.Q.; Li, N.B. Carbon quantum dots prepared with polyethyleneimine as both reducing agent and stabilizer for synthesis of Ag/CQDs composite for Hg<sup>2+</sup> ions detection. *J. Hazard. Mater.* **2017**, *322*, 430–436, doi:10.1016/j.jhazmat.2016.10.034.
108. Ye, Q.; Yan, F.; Luo, Y.; Wang, Y.; Zhou, X.; Chen, L. Formation of N, S-codoped fluorescent carbon dots from biomass and their application for the selective detection of mercury and iron ion. *Spectrochim. Acta A Mol. Biomol. Spectrosc.* **2017**, *173*, 854–862, doi:10.1016/j.saa.2016.10.039.
109. Wang, X.; Yang, X.; Wang, N.; Lv, J.; Wang, H.; Choi, M.M.F.; Bian, W. Graphitic carbon nitride quantum dots as an “off-on” fluorescent switch for determination of mercury(II) and sulfide. *Microchim. Acta* **2018**, *185*, 471, doi:10.1007/s00604-018-2994-0.
110. Bano, D.; Kumar, V.; Singh, V.K.; Hasan, S.H. Green synthesis of fluorescent carbon quantum dots for the detection of mercury(II) and glutathione. *New J. Chem.* **2018**, *42*, 5814–5821, doi:10.1039/C8NJ00432C.
111. Meng, A.; Xu, Q.; Zhao, K.; Li, Z.; Liang, J.; Li, Q. Highly Selective and Sensitive “on-off-on” Fluorescent Probe for Detecting Hg(II) Based on Au/N-doped Carbon Quantum Dots. *Sens. Actuators B Chem.* **2018**, *255*, 657–665, doi:10.1016/j.snb.2017.08.028.
112. Hama Aziz, K.H.; Omer, K.H.; Hamarawfa, R.F. Lowering the detection limit towards nanomolar mercury ion detection via surface modification of N-doped carbon quantum dots. *New J. Chem.* **2019**, *43*, 8677–8683, doi:10.1039/C9NJ01333D.
113. Pourreza, N.; Ghomi, M. Green synthesized carbon quantum dots from *Prosopis juliflora* leaves as a dual off-on fluorescence probe for sensing mercury (II) and chemet drug. *Mater. Sci. Eng. C* **2019**, *98*, 887–896, doi:10.1016/j.msec.2018.12.141.
114. Yahyazadeh, E.; Shemirani, F. Easily synthesized carbon dots for determination of mercury(II) in water samples. *Heliyon* **2019**, *5*, e01596, doi:10.1016/j.heliyon.2019.e01596.
115. Yang, M.; Tang, Q.; Meng, Y.; Liu, J.; Feng, T.; Zhao, X.; Zhu, S.; Yu, W.; Yang, B. Reversible “Off-On” Fluorescence of Zn<sup>2+</sup>-Passivated Carbon Dots: Mechanism and Potential for the Detection of EDTA and Zn<sup>2+</sup>. *Langmuir* **2018**, *34*, 7767–7775, doi:10.1021/acs.langmuir.8b00947.
116. Zhang, Z.; Pei, K.; Yang, Q.; Dong, J.; Yan, Z.; Chen, J. A nanosensor made of sulfur–nitrogen co-doped carbon dots for “off-on” sensing of hypochlorous acid and Zn(II) and its bioimaging properties. *New J. Chem.* **2018**, *42*, 15895–15904, doi:10.1039/C8NJ03159B.
117. Arumugam, N.; Kim, J. Synthesis of carbon quantum dots from Broccoli and their ability to detect silver ions. *Mater. Lett.* **2018**, *219*, 37–40, doi:10.1016/j.matlet.2018.02.043.
118. Cayuela, A.; Soriano, M.L.; Kennedy, S.R.; Steed, J.W.; Valcárcel, M. Fluorescent carbon quantum dot hydrogels for direct determination of silver ions. *Talanta* **2016**, *151*, 100–105, doi:10.1016/j.talanta.2016.01.029.

119. Yu, C.; Qin, D.; Jiang, X.; Zheng, X.; Deng, B. N-doped carbon quantum dots from osmanthus fragrans as a novel off-on fluorescent nanosensor for highly sensitive detection of quercetin and aluminium ion, and cell imaging. *J. Pharm Biomed. Anal.* **2021**, *192*, 113673, doi:10.1016/j.jpba.2020.113673.
120. Radhakrishnan, K.; Panneerselvam, P. Green synthesis of surface-passivated carbon dots from the prickly pear cactus as a fluorescent probe for the dual detection of arsenic(III) and hypochlorite ions from drinking water. *RSC Adv.* **2018**, *8*, 30455–30467, doi:10.1039/C8RA05861J.
121. Raji, K.; Ramanan, V.; Ramamurthy, P. Facile and green synthesis of highly fluorescent nitrogen-doped carbon dots from jack-fruit seeds and its applications towards the fluorimetric detection of Au<sup>3+</sup> ions in aqueous medium and in *in vitro* multicolor cell imaging. *New J. Chem* **2019**, *43*, 11710–11719, doi:10.1039/C9NJ02590A.
122. Yue, J.; Li, L.; Cao, L.; Zhan, M.; Yang, D.; Wang, Z.; Chang, Z.; Mei, Q.; Miao, P.; Dong, W.F. Two-Step Hydrothermal Preparation of Carbon Dots for Calcium Ion Detection. *ACS Appl Mater. Interfaces* **2019**, *11*, 44566–44572, doi:10.1021/acsami.9b13737.
123. Ankireddy, S.R.; Kim, J. Highly Selective and Sensitive Detection of Calcium(II) Ions in Human Serum Using Novel Fluorescent Carbon Dots. *Sens. Actuators B Chem* **2018**, *255*, 3425–3433, doi:10.1016/j.snb.2017.09.172.
124. Niu, W.J.; Shan, D.; Zhu, R.H.; Deng, S.Y.; Cosnier, S.; Zhang, X.J. Dumbbell-Shaped Carbon Quantum Dots/AuNCs Nanohybrid as an Efficient Ratiometric Fluorescent Probe for Sensing Cadmium(II) Ions and L-ascorbic Acid. *Carbon* **2016**, *96*, 1034–1042, doi:10.1016/j.carbon.2015.10.051.
125. Bano, D.; Kumar, V.; Chandra, S.; Kumar Singh, V.; Mohan, S.; Kumar Singh, D.; Talat, M.; Hasan, S.H. Synthesis of highly fluorescent nitrogen-rich carbon quantum dots and their application for the turn-off detection of cobalt (II). *Opt. Mater.* **2019**, *92*, 311–318, doi:10.1016/j.optmat.2019.04.045.
126. Chaudhary, S.; Kumar, S.; Kaura, B.; Mehtaa, S.K. Potential prospects for carbon dots as a fluorescence sensing probe for metal ions. *RSC Adv.* **2016**, *6*, 90526–90536, doi:10.1039/C6RA15691F.
127. Vaz, R.; Bettini, J.; Júnior, J.G.F.; Lima, E.D.S.; Botero, W.G.; Santos, J.C.C.; Schiavon, M.A. High luminescent carbon dots as an eco-friendly fluorescence sensor for Cr(VI) determination in water and soil samples. *J. Photochem. Photobiol. A Chem.* **2017**, *346*, 502–511, doi:10.1016/j.jphotochem.2017.06.047.
128. Rooj, B.; Dutta, A.; Islam, S.; Mandal, U. Green Synthesized Carbon Quantum Dots from *Polygonum tuberosum* L. Petals for Copper (II) and Iron (II) Detection. *J. Fluoresc.* **2018**, *28*, 1261–1267, doi:10.1007/s10895-018-2292-6.
129. Kumari, A.; Kumar, A.; Kumar Sahu, S.; Kumar, S. Synthesis of green fluorescent carbon quantum dots using waste polyolefins residue for Cu<sup>2+</sup> ion sensing and live cell imaging. *Sens. Actuators B Chem.* **2018**, *254*, 197–205, doi:10.1016/j.snb.2017.07.075.
130. Amjadi, M.; Manzoori, J.L.; Hallaj, T.; Azizi, N. Sulfur and nitrogen co-doped carbon quantum dots as the chemiluminescence probe for detection of Cu<sup>2+</sup> ions. *J. Lumin.* **2017**, *182*, 246–251, doi:10.1016/j.jlumin.2016.10.021.
131. Murugan, N.; Prakash, M.; Jayakumar, M.; Sundaramurthy, A.; Sundramoorthy, A.K. Green synthesis of fluorescent carbon quantum dots from *Eleusine coracana* and their application as a fluorescence ‘turn-off’ sensor probe for selective detection of Cu<sup>2+</sup>. *Appl. Surf. Sci.* **2019**, *476*, 468–480, doi:10.1016/j.apsusc.2019.01.090.
132. Gedda, G.; Lee, C.Y.; Lin, Y.C.; Wu, H.F. Green synthesis of Carbon dots from prawn shells for highly selective and sensitive detection of copper ions. *Sens. Actuators B Chem.* **2016**, *224*, 396–403, doi:10.1016/j.snb.2015.09.065.
133. Jayaweera, S.; Yin, K.; Hu, X.; Ng, W.J. Fluorescent N/Al Co-Doped Carbon Dots from Cellulose Biomass for Sensitive Detection of Manganese (VII). *J. Fluoresc.* **2019**, *29*, 1291–1300, doi:10.1007/s10895-019-02452-7.
134. Gong, Y.; Liang, H. Nickel ion detection by imidazole modified carbon dots. *Spectrochim. Acta A Mol. Biomol. Spectrosc.* **2019**, *211*, 342–347, doi:10.1016/j.saa.2018.12.024.
135. Liu, Y.; Zhou, Q.; Yuan, Y.; Wu, Y. Hydrothermal synthesis of fluorescent carbon dots from sodium citrate and polyacrylamide and their highly selective detection of lead and pyrophosphate. *Carbon* **2017**, *115*, 550–560, doi:10.1016/j.carbon.2017.01.035.
136. Hoan, B.T.; Thanh, T.T.; Tam, P.D.; Trung, N.N.; Cho, S.; Pham, V.H. A green luminescence of lemon derived carbon quantum dots and their applications for sensing of V<sup>5+</sup> ions. *Mater. Sci. Eng. B* **2019**, *251*, 114455, doi:10.1016/j.mseb.2019.114455.
137. Chandra, S.; Mahto, T.K.; Chowdhuri, A.R.; Das, B.; Sahu, S.K. One step synthesis of functionalized carbon dots for the ultra-sensitive detection of *Escherichia coli* and iron (III). *Sens. Actuators B Chem.* **2017**, *245*, 835–844, doi:10.1016/j.snb.2017.02.017.
138. Kotta, S.; Aldawsari, H.M.; Badr-Eldin, S.M.; Alhakamy, N.A.; Md, S.; Nair, A.B.; Deb, P.K. Exploring the Potential of Carbon Dots to Combat COVID-19. *Front. Mol. Biosci.* **2020**, *7*, 616575, doi:10.3389/fmolb.2020.616575.
139. Qaddare, S.H.; Salimi, A. Amplified fluorescent sensing of DNA using luminescent carbon dots and AuNPs/GO as a sensing platform: A novel coupling of FRET and DNA hybridization for homogeneous HIV-1 gene detection at femtomolar level. *Biosens. Bioelectron.* **2017**, *89*, 773–780, doi:10.1016/j.bios.2016.10.033.
140. Wang, J.; Lu, T.; Hu, Y.; Wang, X.; Yuangen, Wu. A label-free and carbon dots based fluorescent aptasensor for the detection of kanamycin in milk. *Spectrochim. Acta A Mol. Biomol. Spectrosc.* **2020**, *226*, 117651, doi:10.1016/j.saa.2019.117651.
141. Li, H.; Su, D.; Gao, H.; Yan, X.; Kong, D.; Jin, R.; Liu, X.; Wang, C.; Lu, G. Design of Red Emissive Carbon Dots: Robust Performance for Analytical Applications in Pesticide Monitoring. *Anal. Chem.* **2020**, *92*, 3198–3205, doi:10.1021/acs.analchem.9b04917.
142. Zhao, Y.; Zou, S.; Huo, D.; Hou, D.; Yang, M.; Li, J.; Bian, M. Simple and sensitive fluorescence sensor for methotrexate detection based on the inner filter effect of N, S co-doped carbon quantum dots. *Anal. Chim. Acta* **2019**, *1047*, 179–187, doi:10.1016/j.aca.2018.10.005.
143. Gong, N.H.; Li, Y.L.; Jiang, X.; Zheng, X.F.; Wang, Y.Y.; Huan, S.Y. Fluorescence Resonance Energy Transfer-based Biosensor Composed of Nitrogen-doped Carbon Dots and Gold Nanoparticles for the Highly Sensitive Detection of Organophosphorus Pesticides. *Anal. Sci.* **2016**, *32*, 951–956, doi:10.2116/analsci.32.951.

144. Shen, C.L.; Su, L.X.; Zang, J.H.; Li, X.J.; Lou, Q.; Shan, C.X. Carbon Nanodots as Dual-Mode Nanosensors for Selective Detection of Hydrogen Peroxide. *Nanoscale Res. Lett.* **2017**, *12*, 447, doi:10.1186/s11671-017-2214-6.
145. Liang, N.; Hu, X.; Li, W.; Mwakosya, A.W.; Guo, Z.; Xu, Y.; Huang, X.; Li, Z.; Zhang, X.; Zou, X.; et al. Fluorescence and colorimetric dual-mode sensor for visual detection of malathion in cabbage based on carbon quantum dots and gold nanoparticles. *Food Chem.* **2021**, *343*, 128494, doi:10.1016/j.foodchem.2020.128494.
146. Zhu, Y.; Lu, Y.; Shi, L.; Yang, Y.  $\beta$ -Cyclodextrin functionalized N,Zn codoped carbon dots for specific fluorescence detection of fluoroquinolones in milk samples. *Microchem. J.* **2020**, *153*, 104517, doi:10.1016/j.microc.2019.104517.
147. Das, P.; Ganguly, S.; Mondal, S.; Bose, M.; Kumar Das, A.; Banerjee, S.; Das, N.C. Heteroatom doped photoluminescent carbon dots for sensitive detection of acetone in human fluids. *Sens. Actuators B Chem.* **2018**, *266*, 583–593, doi:10.1016/j.snb.2018.03.183.
148. Zhang, Q.Q.; Chen, B.B.; Zou, H.Y.; Li, Y.F.; Huang, C.Z. Inner filter with carbon quantum dots: A selective sensing platform for detection of hematin in human red cells. *Biosens. Bioelectron.* **2018**, *100*, 148–154, doi:10.1016/j.bios.2017.08.049.
149. Mandal, P.; Sahoo, D.; Sarkar, P.; Chakraborty, K.; Das, S. Fluorescence turn-on and turn-off sensing of pesticides by carbon dot-based sensor. *New J. Chem.* **2019**, *43*, 12137–12151, doi:10.1039/C9NJ03192H.
150. Wang, K.; Ji, Q.; Xu, J.; Li, H.; Zhang, D.; Liu, X.; Wu, Y.; Fan, H. Highly Sensitive and Selective Detection of Amoxicillin Using Carbon Quantum Dots Derived from Beet. *J. Fluoresc.* **2018**, *28*, 759–765, doi:10.1007/s10895-018-2237-0.
151. Wang, R.; Wang, X.; Sun, Y. Aminophenol-based carbon dots with dual wavelength fluorescence emission for determination of heparin. *Microchim. Acta* **2017**, *184*, 187–193, doi:10.1007/s00604-016-2009-y.
152. Achadu, O.J.; Takemura, K.; Khoris, I.M.; Park, E.Y. Plasmonic/magnetic molybdenum trioxide and graphitic carbon nitride quantum dots-based fluoroimmunosensing system for influenza virus. *Sens. Actuators B Chem.* **2020**, *15*, 128494, doi:10.1016/j.snb.2020.128494.
153. Xu, L.-D.; Zhang, Q.; Ding, S.-N.; Xu, J.-J.; Chen, H.-Y. Ultrasensitive Detection of Severe Fever with Thrombocytopenia Syndrome Virus Based on Immunofluorescent Carbon Dots/SiO<sub>2</sub> Nanosphere-Based Lateral Flow Assay. *ACS Omega* **2019**, *4*, 21431–21438, doi:10.1021/acsomega.9b03130.
154. Anju; Rais, A.; Rawat, K.; Prasad, T.; Bohidar, H.B. Boron-doped carbon quantum dots: A 'turn-off' fluorescent probe for dopamine detection. *Nanotechnology* **2020**, *32*, 025501, doi:10.1088/1361-6528/abb84d.
155. Song, Z.; Quan, F.; Xu, Y.; Liu, M.; Cui, L.; Liu, J. Multifunctional N,S co-doped carbon quantum dots with pH- and thermo-dependent switchable fluorescent properties and highly selective detection of glutathione. *Carbon* **2016**, *104*, 169–178, doi:10.1016/j.carbon.2016.04.003.
156. Issa, M.A.; Abidin, Z.Z.; Sobri, S.; Rashid, S.; Mahdi, M.A.; Ibrahim, N.A.; Pudza, M.Y. Facile Synthesis of Nitrogen-Doped Carbon Dots from Lignocellulosic Waste. *Nanomaterials* **2019**, *9*, 1500, doi:10.3390/nano9101500.
157. Zhang, Y.; Fang, X.; Zhao, H.; Li, Z. A highly sensitive and selective detection of Cr(VI) and ascorbic acid based on nitrogen-doped carbon dots. *Talanta* **2018**, *181*, 318–325, doi:10.1016/j.talanta.2018.01.027.
158. Loo, A.H.; Sofer, Z.; Bouša, D.; Ulbrich, P.; Bonanni, A.; Pumera, M. Carboxylic Carbon Quantum Dots as a Fluorescent Sensing Platform for DNA Detection. *ACS Appl. Mater. Interfaces* **2016**, *8*, 1951–1957, doi:10.1021/acsmi.5b10160.
159. Li, J.; Li, X.; Weng, R.; Qiang, T.; Wang, W. Glucose assay based on a fluorescent multi-hydroxyl carbon dots reversible assembly with phenylboronic acid brush grafted magnetic nanoparticles. *Sens. Actuators B Chem.* **2020**, *304*, 127349, doi:10.1016/j.snb.2019.127349.
160. Yan, F.; Zu, F.; Xu, J.; Zhou, X.; Bai, Z.; Ma, C.; Luo, Y.; Chen, L. Fluorescent carbon dots for ratiometric detection of curcumin and ferric ion based on inner filter effect, cell imaging and PVDF membrane fouling research of iron flocculants in wastewater treatment. *Sens. Actuators B Chem.* **2019**, *287*, 231–240, doi:10.1016/j.snb.2019.01.144.
161. Jung Lai, I.; Harroun, S.G.; Chen, S.Y.; Unnikrishnan, B.; Li, Y.J.; Huang, C.C. Solid-state synthesis of self-functional carbon quantum dots for detection of bacteria and tumor cells. *Sens. Actuators B Chem.* **2016**, *228*, 465–470, doi:10.1016/j.snb.2016.01.062.
162. Wang, B.; Chen, Y.; Wu, Y.; Weng, B.; Liu, Y.; Lu, Z.; Li, C.M.; Yu, C. Aptamer induced assembly of fluorescent nitrogen-doped carbon dots on gold nanoparticles for sensitive detection of AFB<sub>1</sub>. *Biosens. Bioelectron.* **2016**, *78*, 23–30, doi:10.1016/j.bios.2015.11.015.
163. Devi, N.R.; Vignesh Kumar, T.H.; Sundramoorthy, A.K. Electrochemically Exfoliated Carbon Quantum Dots Modified Electrodes for Detection of Dopamine Neurotransmitter. *J. Electrochem. Soc.* **2018**, *165*, doi:10.1149/2.0191812jes.
164. Li, X.; Zhao, Z.; Pan, C. Ionic liquid-assisted electrochemical exfoliation of carbon dots of different size for fluorescent imaging of bacteria by tuning the water fraction in electrolyte. *Microchim. Acta* **2016**, *183*, 2525–2532, doi:10.1007/s00604-016-1877-5.
165. Zeng, L.; Li, X.; Fan, S.; Li, J.; Mu, J.; Qin, M.; Wang, L.; Gan, G.; Tadé, M.; Liu, S. The bioelectrochemical synthesis of high-quality carbon dots with strengthened electricity output and excellent catalytic performance. *Nanoscale* **2019**, *11*, 4428–4437, doi:10.1039/C8NR10510C.
166. Zhao, Z.; Xie, Y. Enhanced electrochemical performance of carbon quantum dots-polyaniline hybrid. *J. Power Sources* **2016**, *337*, 54–64, doi:10.1016/j.jpowsour.2016.10.110.

167. Niu, F.; Xu, A.; Liu, J.; Song, Z.; Liu, M.; Liu, J. Controllable electrochemical/electroanalytical approach to generate nitrogen-doped carbon quantum dots from varied amino acids: Pinpointing the utmost quantum yield and the versatile photoluminescent and electrochemiluminescent applications. *Electrochim. Acta* **2017**, *236*, 239–251, doi:10.1016/j.electacta.2017.03.085.
168. Tan, S.C.; Chin, S.F.; Pang, S.C. Disposable carbon dots modified screen printed carbon electrode electrochemical sensor strip for selective detection of ferric ions. *J. Sens.* **2017**, *2017*, 7576345, doi:10.1155/2017/7576345.
169. Fares, N.V.; Medhat, P.M.; El Maraghy, C.M.; Okeil, S.; Ayad, M.F. Influence of Nitrogen-Doped Carbon Dot and Silver Nanoparticle Modified Carbon Paste Electrodes on the Potentiometric Determination of Tobramycin Sulfate: A Comparative Study. *Chemosensors* **2021**, *9*, 52, doi:10.3390/chemosensors9030052.
170. Algarra, M.; González-Calabuig, A.; Radotić, K.; Mutavdzic, D.; Ania, C.; Lázaro-Martínez, J.; Jiménez-Jiménez, J.; Rodríguez-Castellón, E.; del Valle, M. Enhanced electrochemical response of carbon quantum dot modified electrodes. *Talanta* **2018**, *178*, 679–685, doi:10.1016/j.talanta.2017.09.082.
171. Pandey, P.K.; Preeti; Rawat, K.; Prasad, T.; Bohidar, H.B. Ultrasensitive Detection of Severe Fever with Thrombocytopenia Syndrome Virus Based on Immunofluorescent Carbon Dots/SiO<sub>2</sub> Nanosphere-Based Lateral Flow Assay. *J. Mater. Chem. B* **2020**, *8*, 1277–1289, doi:10.1039/C9TB01863H.
172. Sharath Shankar, S.; Shreema, R.; Ramachandran, V.; Sruthi, T.V.; Sameer Kumar, V.B.; Rakhi, R.B. Carbon Quantum Dot-Modified Carbon Paste Electrode-Based Sensor for Selective and Sensitive Determination of Adrenaline. *ACS Omega* **2019**, *4*, 7903–7910, doi:10.1021/acsomega.9b00230.
173. Wei, Y.; Zhang, D.; Fang, Y.; Wang, H.; Liu, Y.; Xu, Z.; Wang, S.; Guo, Y. Detection of Ascorbic Acid Using Green Synthesized Carbon Quantum Dots. *J. Sens.* **2019**, *2019*, 1–10, doi:10.1155/2019/9869682.